

Light-induced Faraday effect from dynamical breakdown of Kleinman symmetry

Niccolò Sellati,^{1,*} Jacopo Fiore,^{1,2} and Lara Benfatto^{1,†}

¹*Department of Physics, “Sapienza” University of Rome, P.le A. Moro 5, 00185 Rome, Italy*

²*Institute for Theory of Statistical Physics, RWTH Aachen University, Aachen, Germany*

(Dated: May 27, 2026)

The observation of anomalously large polarization rotations in pump-probe experiments with circularly polarized light has recently challenged the conventional understanding of the inverse Faraday effect. The striking magnitude of these responses implies the generation of effective magnetic fields orders of magnitude larger than theoretical expectations, raising fundamental questions about the nature of light-induced time-reversal symmetry breaking. In this work we demonstrate that a static polarization rotation can originate entirely from the antisymmetric component of the third-order optical susceptibility, without generating a macroscopic magnetization of the material. We show that this light-induced Faraday effect is inherently dynamical, emerging when Kleinman symmetry breaks down. Using a minimal *sp* tight-binding model on a square lattice, we demonstrate that the light-induced Faraday response can be sizable even far from dissipative resonances. While the effect emerges at a purely electronic level, we show that resonant coupling with phonons can significantly enhance the pump-probe response.

I. INTRODUCTION

The Faraday effect is a paradigmatic manifestation of time-reversal symmetry breaking, observed as the polarization rotation of light propagating through a medium in the presence of either an external static magnetic field H^z or spontaneous magnetic order [1–4]. For a monochromatic electric field with polarization vector \mathcal{E} , this effect is captured by the free-energy contribution [1]

$$F = -i\chi^{(F)}H^z(\mathcal{E} \times \mathcal{E}^*)_z = \chi^{(F)}H^z(|\mathcal{E}_L|^2 - |\mathcal{E}_R|^2), \quad (1)$$

where $\chi^{(F)}$ is the Faraday susceptibility. In transparent media, $\chi^{(F)}$ is a real quantity governing the splitting of the refractive index n for left- (\mathcal{E}_L) and right-circularly (\mathcal{E}_R) polarized light, $n_{L/R} = n \pm 2\pi\chi^{(F)}H^z/n$. Large Faraday rotations are typically driven by spontaneous magnetization or strong spin-orbit coupling in magnetic systems [5]. However, non-magnetic materials can also exhibit a small but finite $\chi^{(F)}$, arising from non-resonant electronic excitations [6].

The advent of phase-stable, high-intensity light sources has sparked considerable interest in optomagnetic effects [7], where magnetic properties are manipulated via optical pulses. While strong effects are expected primarily in magnetic media, recent experiments in paramagnetic materials driven by circularly polarized pulses [8–10] have challenged this picture. These studies rely on the inverse Faraday effect (IFE), described by the same free-energy of Eq. (1), to induce a static magnetization $M^z = -\partial F/\partial H^z \propto |\mathcal{E}_L|^2 - |\mathcal{E}_R|^2$ in the material. The resulting magnetization is typically detected through the polarization rotation of a delayed probe pulse [8, 9]. Despite the weak paramagnetic nature of the driven systems, the observed response is remarkably large, raising

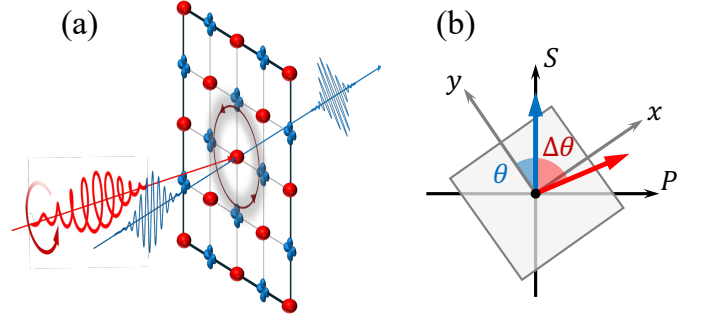


Figure 1. (a) Schematic illustration of the light-induced Faraday effect: a circularly polarized pump induces a collective electronic response, resulting in a rotation of the probe polarization. (b) Polarization geometry. The probe (blue) defines a fixed PS reference frame, while the sample is rotated by an angle θ . The pump (red) is described in a reference frame rotated by a fixed angle $\Delta\theta$ with respect to PS .

fundamental questions about its microscopic origin. For pumps in the visible range, evidence suggests that the IFE is not governed by the same magneto-optical constant $\chi^{(F)}$ that controls the direct Faraday effect [8], even though the reciprocity between the two processes was established long ago through direct measurements of M^z outside the sample [2]. In the terahertz (THz) regime, experiments resonantly driving soft infrared-active phonons have explored whether the large Faraday rotation originates from ionic magnetic moments. Dynamical multiferroicity [11–14] predicts that circular lattice motion generates an ionic magnetization able to induce a probe rotation through the direct Faraday effect. However, the corresponding magnetization inferred from the experimental rotation angle [9] exceeds *ab initio* estimates by several orders of magnitude. This discrepancy has sparked intense theoretical efforts aimed at explaining the anomalously large vibrational magnetism [15–19]. Alternative approaches instead suggest that circular driving gener-

* niccolo.sellati@uniroma1.it

† lara.benfatto@roma1.infn.it

ates transient, non-Maxwellian magnetic-like fields confined within the material, thereby remaining inaccessible to external magnetic probes [20, 21].

In this manuscript, we resolve the apparent inconsistency between theory and experimental observations by attributing the anomalous optical response to a light-induced Faraday effect, sketched in Fig. 1(a). This phenomenon emerges directly from the third-order optical susceptibility $\chi_{ij;kl}$ and, crucially, does not induce a real macroscopic magnetization of the sample. By exploiting the intimate connection between the frequency dependence and the spatial symmetries of $\chi_{ij;kl}$ [1, 22], we decompose the total response into symmetric and antisymmetric components $\chi_{xy}^{S,A}$ with respect to the frequencies of the pump fields. While the former generates the optical Kerr effect [23], observable also with linearly polarized light, the light-induced Faraday effect is governed by the antisymmetric component χ_{xy}^A , and only emerges under circularly polarized driving. The corresponding free-energy contribution can be expressed as

$$F = -\chi_{xy}^A (\mathbf{E}_{\text{pu}} \times \mathbf{E}_{\text{pu}}^*)_z (\mathbf{E}_{\text{pr}} \times \mathbf{E}_{\text{pr}}^*)_z, \quad (2)$$

where \mathbf{E}_{pu} and \mathbf{E}_{pr} denote the pump and probe polarization vectors, respectively. The link to the magneto-optical Faraday effect described by Eq. (1) becomes evident by identifying the circularly polarized pump as an effective time-reversal-breaking field. A key observation is that under the static approximation Kleinman symmetry holds [22], forcing the antisymmetric component to vanish. The light-induced Faraday effect thus represents a purely dynamical response that emerges when Kleinman symmetry is broken at finite frequencies, even far from dissipative resonances. This fundamental symmetry constraint explains why previous theoretical estimates [8, 9], based on a static approximation for $\chi_{ij;kl}$, could not capture the light-induced Faraday response and therefore motivated interpretations based on alternative mechanisms.

To quantitatively estimate the magnitude of the light-induced Faraday effect, we compute the relative strength of χ_{xy}^A and χ_{xy}^S within a multi-orbital toy model. The resulting response is of the same order of magnitude as that observed in Ref. [9] for paraelectric SrTiO₃. Notably, while the light-induced Faraday effect is intrinsically present at the purely electronic level, the resonant driving of infrared-active phonons can significantly enhance the response. In SrTiO₃, the softening of the phonon mode at low temperatures naturally accounts for the measured temperature dependence of the light-induced Faraday response, as we demonstrate by explicitly computing the lattice contribution to the dynamical antisymmetric response.

The mechanism behind the light-induced Faraday effect is fundamentally distinct from the IFE, as it does not involve the generation of a magnetization or external magnetic fields. Instead, the light-induced effect exploits the explicit time-reversal symmetry breaking of circularly polarized light to drive intrinsically dynamical nonlinear

processes, the magnitude of which cannot be captured by static considerations. Our findings suggest that these dynamical effects are a general feature of transparent media, challenging the common assumption that a static description based on Kleinman symmetry provides an adequate picture of the nonlinear response of wide-bandgap insulators.

II. STATIC ANTISYMMETRIC RESPONSE

Connecting the light-induced Faraday effect to experimentally observable signals requires a careful modeling of the pump-probe balanced-detection setup, analogous to that employed in Refs. [9, 23]. The incoming probe field defines the PS reference frame, with the S axis aligned with the probe polarization $E_{\text{pr}}(\omega)$ [Fig. 1(b)]. In this geometry, a pump-induced probe rotation generates a nonlinear electric field along the orthogonal P axis, arising from the nonlinear polarization component P_{NL}^P . The resulting signal is recorded using a balanced-detection scheme [24] as a function of the pump-probe time delay t_{pp} , and the measured quantity $\Delta\Gamma(t_{pp})$, corresponding to the differential intensity between the two photodiodes, is directly proportional to P_{NL}^P , as shown in Ref. [23]. For simplicity, we here assume that the PS frame coincides with the crystallographic xy axes of the cubic crystal. The more general case of a finite rotation angle θ between the two frames is discussed in the Supplemental Material [25]. In this configuration, the incoming probe is polarized along y , and the differential signal is proportional to the x component of the nonlinear polarization. In particular, for third-order nonlinearities [22, 23, 26],

$$\begin{aligned} \Delta\Gamma(t_{pp}) \propto P_{\text{NL}}^x = & 3 \sum_{l \neq k} \int d\omega_1 d\omega_2 d\omega_3 e^{-i(\omega_2 + \omega_3)t_{pp}} \\ & \times \chi_{xy;kl}(\omega; \omega_1, \omega_2, \omega_3) E_{\text{pr}}(\omega_1) E_{\text{pu}}^k(\omega_2) E_{\text{pu}}^l(\omega_3), \quad (3) \end{aligned}$$

where $k, l = x, y$. The four-wave-mixing processes generate sidebands around the fundamental probe frequency ω_1 , shifted by $\omega_2 + \omega_3$, which appear as temporal modulations of $\Delta\Gamma(t_{pp})$. Here, $E_{\text{pu}}^{k,l}$ denote the x or y components of the pump field, polarized at an angle $\Delta\theta$ with respect to the probe at $t_{pp} = 0$. For the third-order susceptibility $\chi_{ij;kl}(\omega_i; \omega_j, \omega_k, \omega_l)$ we adopt the standard convention in which i labels the outgoing nonlinear signal, j the incoming probe, and k, l the pump fields. Energy conservation fixes $\omega_i = \omega_j + \omega_k + \omega_l$. Eq. (3) assumes that all possible generated sidebands of the probe are collected by the photodetectors.

In this notation, each spatial index s is associated with a corresponding frequency ω_s . While intrinsic permutation symmetry ensures that the susceptibility remains unchanged under a simultaneous swap of spatial indices and their associated frequencies [22], $\chi_{xy;kl}(\omega; \omega_1, \omega_2, \omega_3) = \chi_{xy;lk}(\omega; \omega_1, \omega_3, \omega_2)$, exchanging only the spatial indices while keeping the frequencies fixed generally yields inequivalent tensor components

$\chi_{xy;kl}(\omega; \omega_1, \omega_2, \omega_3) \neq \chi_{xy;lk}(\omega; \omega_1, \omega_2, \omega_3)$. In the static limit, however, this distinction disappears and one recovers $\chi_{xy;kl}(0; 0, 0, 0) = \chi_{xy;lk}(0; 0, 0, 0)$. This property, known as Kleinman symmetry [22], is often assumed to remain valid in dynamical conditions, provided that all optical frequencies lie below the electronic band gap. The underlying assumption is that, in the transparent regime, the material response is effectively instantaneous and non-adiabatic effects are negligible. However, the static approximation is fundamentally inadequate for describing the response under circularly polarized driving, and leads to qualitatively wrong results. To show that this is the case, we take advantage of the permutation symmetry of the susceptibility and recast Eq. (3) as $\Delta\Gamma(t_{pp}) \propto \int d\omega_1 d\omega_2 d\omega_3 e^{-i(\omega_2 + \omega_3)t_{pp}} E_{pr}(\omega_1) \Delta\gamma(\omega_1, \omega_2, \omega_3)$, where

$$\begin{aligned} \Delta\gamma(\omega_1, \omega_2, \omega_3) &= \chi_{xy}^A(\omega; \omega_1, \omega_2, \omega_3) \mathcal{A} \\ &+ \chi_{xy}^S(\omega; \omega_1, \omega_2, \omega_3) (\sin(2\Delta\theta) \mathcal{S}_{\parallel} + \cos(2\Delta\theta) \mathcal{S}_{\perp}). \end{aligned} \quad (4)$$

Here, $\mathcal{S}_{\parallel, \perp}$ and \mathcal{A} denote combinations of the pump-field components that are, respectively, symmetric and antisymmetric under exchange $\omega_2 \leftrightarrow \omega_3$,

$$\begin{aligned} \mathcal{S}_{\parallel} &= E_{pu}^y(\omega_2) E_{pu}^y(\omega_3) - E_{pu}^x(\omega_2) E_{pu}^x(\omega_3), \\ \mathcal{S}_{\perp} &= E_{pu}^x(\omega_2) E_{pu}^y(\omega_3) + E_{pu}^y(\omega_2) E_{pu}^x(\omega_3), \\ \mathcal{A} &= E_{pu}^x(\omega_2) E_{pu}^y(\omega_3) - E_{pu}^y(\omega_2) E_{pu}^x(\omega_3). \end{aligned} \quad (5)$$

The coefficients χ_{xy}^S and χ_{xy}^A represent, analogously, symmetric and antisymmetric combinations of the susceptibility components,

$$\begin{aligned} \chi_{xy}^{S,A}(\omega; \omega_1, \omega_2, \omega_3) &= \chi_{xy;xy}(\omega; \omega_1, \omega_2, \omega_3) \\ &\pm \chi_{xy;yx}(\omega; \omega_1, \omega_2, \omega_3). \end{aligned} \quad (6)$$

It is evident that the antisymmetric contribution to the differential signal would vanish under Kleinman symmetry, while the symmetric terms remain finite.

For a circularly polarized pump, the symmetric and antisymmetric components of the susceptibility give rise to oscillations at distinct frequencies in $\Delta\Gamma(t_{pp})$. This separation becomes evident for a monochromatic pump at frequency Ω , where the field components $E_{pu}^{x,y}(\omega_s) = \mathcal{E}_{x,y} \delta(\omega_s - \Omega) + \mathcal{E}_{x,y}^* \delta(\omega_s + \Omega)$ can be expressed in the circular basis through $\mathcal{E}_{L,R} = (\mathcal{E}_x \pm i\mathcal{E}_y)/\sqrt{2}$. By using this decomposition in Eq. (4) we see that the symmetric field combinations generate oscillations at $\pm 2\Omega$, whereas the antisymmetric component generates a static response. By Fourier transforming the differential signal with respect to the pump-probe delay, $\Delta\Gamma(t_{pp}) \rightarrow \Delta\bar{\Gamma}(\omega_{pp})$, and taking a monochromatic probe at frequency ω , the second-harmonic response reads

$$\begin{aligned} \Delta\bar{\Gamma}(2\Omega) &\sim \chi_{xy}^S(\omega + 2\Omega; \omega, \Omega, \Omega) \left[\sin(2\Delta\theta) (\mathcal{E}_L^2 + \mathcal{E}_R^2) \right. \\ &\left. + i \cos(2\Delta\theta) (\mathcal{E}_L^2 - \mathcal{E}_R^2) \right]. \end{aligned} \quad (7)$$

An analogous expression is found for the negative-frequency component, with complex conjugate projectors. These two contributions describe the optical Kerr

effect [23]. On the other hand, the static response takes the form

$$\begin{aligned} \Delta\bar{\Gamma}(0) &\sim \chi_{xy}^A(\omega; \omega, \Omega, -\Omega) (\mathcal{E} \times \mathcal{E}^*)_z = \\ &= i\chi_{xy}^A(\omega; \omega, \Omega, -\Omega) (|\mathcal{E}_L|^2 - |\mathcal{E}_R|^2), \end{aligned} \quad (8)$$

where $\mathcal{E} = (\mathcal{E}_x, \mathcal{E}_y)$, and we used the identity $\mathcal{E}_x \mathcal{E}_y^* - \mathcal{E}_x^* \mathcal{E}_y = i(|\mathcal{E}_L|^2 - |\mathcal{E}_R|^2)$. We note that this contribution is finite even for a purely real χ_{xy}^A , as typically realized when both pump and probe frequencies lie below the electronic band gap. Because $\mathcal{E} \rightarrow \mathcal{E}^*$ under time reversal, the field combination $(\mathcal{E} \times \mathcal{E}^*)_z$ explicitly breaks time-reversal symmetry. Consequently, the contribution in Eq. (8) can be interpreted as a light-induced Faraday effect, in which the finite-frequency circularly polarized pump plays the same role as the external magnetic field H^z in the conventional magneto-optical Faraday effect described by Eq. (1). The key difference is that the light-induced mechanism involves an effective fictitious magnetic field [20, 21], that rotates the probe polarization without generating a macroscopic magnetization.

To isolate helicity-dependent contributions, the standard experimental procedure [9] is to consider the dichroic signal $\Delta\bar{\Gamma}_{R-L}(\omega_{pp}) = \frac{1}{2} [\Delta\bar{\Gamma}_R(\omega_{pp}) - \Delta\bar{\Gamma}_L(\omega_{pp})]$, defined as the difference between the pump-probe response to right ($\Delta\Gamma_R$) and left ($\Delta\Gamma_L$) polarized light. In addition to the time-reversal breaking static response, the dichroic signal also contains a 2Ω component arising from the helicity-odd term proportional to $\mathcal{E}_L^2 - \mathcal{E}_R^2$ in Eq. (7), and a -2Ω component from its complex conjugate.

To correctly interpret the experimental spectra as the ones of Ref. [9], one must also account for a finite frequency mismatch $\Delta\Omega$ between the pump components $E_{pu}^x(\omega_s)$ and $E_{pu}^y(\omega_s)$. As discussed in the Supplemental Material [25], such a mismatch shifts the light-induced Faraday response to finite frequency $\Delta\Omega$, while simultaneously activating an additional contribution from the symmetric channel at the same frequency. The latter coincides with the quasi-static signal discussed in Refs. [9, 23] under the assumption of Kleinman symmetry. As a consequence, the experimentally observed quasi-static response generally contains contributions from both channels. We note that recent theoretical works [15, 16, 20, 21] did not explicitly include the contribution of the symmetric channel to the quasi-static peak at $\Delta\Omega$, which may have led to an overestimate of the apparently anomalous signal. Within the present framework, the full spectrum instead emerges naturally from the interplay between Kerr and light-induced Faraday responses. On the experimental side, the two contributions can in principle be disentangled through angle-resolved measurements. Indeed, the antisymmetric response is entirely independent of the probe polarization angle θ [25], whereas the symmetric contribution displays the characteristic fourfold angular dependence discussed in Ref. [23].

Finally, we note that for a linearly polarized pump both the static and the oscillatory $\pm 2\Omega$ components originate

entirely from the symmetric terms of Eq. (4), while the antisymmetric contribution vanishes as $(\boldsymbol{\mathcal{E}} \times \boldsymbol{\mathcal{E}}^*)_z = 0$ [25]. In this case, a theoretical description based on Kleinman symmetry is sufficient to reproduce all qualitative features of the experimental response, as demonstrated in Ref. [23].

III. MICROSCOPIC ESTIMATE OF THE DYNAMICAL ELECTRONIC RESPONSE

The emergence of the static light-induced Faraday effect under circular driving, encoded in Eq. (8), is a general consequence of the dynamical breakdown of Kleinman symmetry. Evaluating the relevance of this mechanism for the experimental observations, however, requires a quantitative estimate of the relative magnitude of the antisymmetric and symmetric susceptibilities, χ_{xy}^A/χ_{xy}^S . Since the latter uniquely determines the Kerr response at 2Ω as given by Eq. (7), this ratio provides a natural measure of the strength of the light-induced Faraday contribution. Because the susceptibilities depend sensitively on the underlying electronic transitions, a realistic description would require a detailed microscopic modeling of the full band structure. Here, rather than addressing a specific material, we employ a minimal toy model designed to identify the microscopic ingredients responsible for a sizable antisymmetric susceptibility in both resonant and off-resonant regimes.

As will become clear in the following, distinct orbital characters of valence and conduction bands give rise to additional microscopic channels contributing to the antisymmetric susceptibility, thereby enhancing the light-induced Faraday effect. As a representative multiorbital toy model we then consider a square lattice with two atoms per unit cell, A and B, hosting s - and $p_{x,y}$ -type orbitals, respectively. We include nearest-neighbor hopping with amplitude t , and assign on-site energies $\mp\Delta$ to the two sublattices. The real-space structure of the model is shown in Fig. 2(a), while the corresponding band structure is reported in Fig. 2(b). The lower band $E_1(\mathbf{k})$, shown in red, is predominantly s -like, whereas the upper bands $E_2(\mathbf{k})$ and $E_3(\mathbf{k})$, in blue, are mainly of p -like character and degenerate at the Γ -point. Here, a direct 2Δ gap is present. In the following we set the chemical potential such that $E_1(\mathbf{k})$ is the valence band. $E_3(\mathbf{k})$ is flat throughout the Brillouin zone, as a consequence of restricting the hopping to nearest neighbors.

The light-matter interaction is introduced via the Peierls substitution $\mathbf{k} \rightarrow \mathbf{k} + e\mathbf{A}/c$ in the tight-binding Hamiltonian $\mathcal{H}_{\mathbf{k}}$, where $-e$ is the electron charge, c the speed of light and \mathbf{A} the vector potential describing the optical perturbation. As detailed in the Supplemental Material [25], we derive the effective quantum action for the electronic system in the presence of the electromagnetic field by expanding the Hamiltonian in powers of \mathbf{A} and integrating out the electronic degrees of freedom [27, 28]. This procedure yields the microscopic counter-

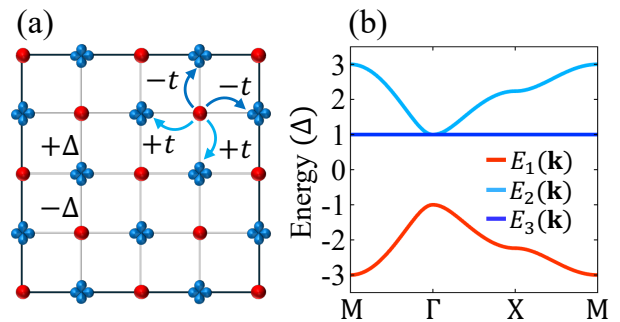


Figure 2. (a) Real-space structure of the square sp -model. Each unit cell contains two sites: site A hosting an s -type orbital (red) and site B hosting $p_{x,y}$ -type orbitals (blue). The two sublattices have on-site energies $-\Delta$ and $+\Delta$ respectively, and are connected by nearest-neighbor hopping with amplitude t . (b) Band structure along high-symmetry directions of the Brillouin zone for $t/\Delta = 1$. The red band has predominant s -like orbital character, the blue bands have p -like character.

part of the free-energy in Eq. (2), where the third-order nonlinear response is mediated by electronic transitions. The corresponding contributions are shown in Fig. 3(a), each diagram defining a third-order nonlinear kernel. For clarity, we present the expressions for a monochromatic pump, while the generalization to fields with finite bandwidth is straightforward.

We first consider a diamagnetic-like contribution, in which light-matter coupling occurs through two-photon excitation processes mediated by the density-like vertex $\rho_i = \partial^2 \mathcal{H}_{\mathbf{k}} / \partial k_i^2$. Denoting with $[\rho_i]_{ab}$ the matrix element of the electronic transitions between bands a and b , the resulting antisymmetric kernel scales as [25]

$$\begin{aligned} \mathbf{K}_{\text{dia}}^A(\omega; \omega, \Omega, -\Omega) &\sim \sum_{ab} [[\rho_x]_{ab}[\rho_y]_{ba} + [\rho_y]_{ab}[\rho_x]_{ba}] \\ &\times [d_{ab}(\omega - \Omega) - d_{ab}(\omega + \Omega)]. \end{aligned} \quad (9)$$

Here, the function d_{ab} collects the frequency-dependent poles associated with electronic transitions, and is independent of the Cartesian indices. The diamagnetic kernel already illustrates why the antisymmetric response becomes finite at finite frequency: the two terms $\mathbf{K}_{xy;xy}^{\text{dia}}(\omega; \omega, \Omega, -\Omega)$ and $\mathbf{K}_{xy;yx}^{\text{dia}}(\omega; \omega, \Omega, -\Omega)$ that compose $\mathbf{K}_{\text{dia}}^A$ explore different intermediate states after the first transition driven by the y -polarized pump and probe photons, as sketched in Fig. 3(b). In the former, the y -polarized pump carries frequency $-\Omega$, such that the intermediate state evolves with $\omega - \Omega$. In the latter, it instead carries Ω , yielding an intermediate state at $\omega + \Omega$. This dynamical dephasing between the two processes produces a finite difference between the corresponding kernels and therefore a nonvanishing antisymmetric response.

The paramagnetic-like contribution, on the other hand, corresponds to processes involving one-photon excitations only, with four velocity vertices $v_i = \partial \mathcal{H}_{\mathbf{k}} / \partial k_i$.

Introducing the velocity vector $\mathbf{v} = (v_x, v_y)$, the corresponding antisymmetric kernel can be expressed in a compact form as [25]

$$\begin{aligned} K_{\text{para}}^A(\omega; \omega, \Omega, -\Omega) &\sim \sum_{abcd} [([\mathbf{v}]_{ab} \times [\mathbf{v}]_{bc}) \cdot ([\mathbf{v}]_{cd} \times [\mathbf{v}]_{da})] \\ &\times [p_{abcd}(-\Omega, \Omega, \omega) - p_{abcd}(\Omega, -\Omega, \omega)] + \text{perm.}, \quad (10) \end{aligned}$$

where the function p_{abcd} plays the same role as d_{ab} for paramagnetic-like transitions, and ‘‘perm.’’ accounts for all permutations of the pump-probe interaction sequence. Eq. (10) also highlights the importance of a multi-orbital electronic structure for obtaining a finite antisymmetric paramagnetic response, as also pointed out for the antisymmetric Raman response in Ref. [29]. In effective two-band models derived from a single orbital channel, the velocity matrix elements are not independent and instead become proportional to each other by symmetry. As a consequence, the corresponding cross products vanish identically, suppressing the paramagnetic contribution. Finally, the mixed paramagnetic-diamagnetic contribution corresponds to processes involving both one- and two-photon excitations, leading to the kernel $K_{\text{mix}}^A(\omega; \omega, \Omega, -\Omega)$. Its explicit expression, lengthier but analogous to the previous terms, is reported in the Supplemental Material [25].

By expressing the electric field in terms of the time derivative of the gauge potential, the full antisymmetric susceptibility can be obtained from the corresponding nonlinear kernels as $\chi_{xy}^A = [K_{\text{dia}}^A + K_{\text{para}}^A + K_{\text{mix}}^A]/(\omega^2 \Omega^2)$, where the frequency dependence has been left implicit for compactness. The resulting susceptibility scales linearly with both pump and probe frequencies in the low-frequency limit,

$$\chi_{xy}^A(\omega; \omega, \Omega, -\Omega) \sim \omega \Omega \quad \text{for } \omega, \Omega \rightarrow 0. \quad (11)$$

This demonstrates that the light-induced Faraday effect is intrinsically dynamical and requires finite-frequency pump and probe fields. Analogous calculations yield the symmetric susceptibility χ_{xy}^S which, as expected for a wide-bandgap insulator, remains finite in the static limit $\omega, \Omega \rightarrow 0$.

To quantitatively estimate the relative magnitude of the antisymmetric and symmetric susceptibilities within the sp -model, we compute the ratio $\chi_{xy}^A(\omega; \omega, \Omega, -\Omega)/\chi_{xy}^S(\omega; \omega, \Omega, -\Omega)$ as a function of the pump and probe frequencies Ω and ω , and show the result in Fig. 3(c). While both susceptibilities increase upon approaching the band gap, the antisymmetric contribution grows comparatively faster, leading to a strong enhancement of the ratio near resonance. Remarkably, a sizable antisymmetric susceptibility persists even far from the resonance condition. By fixing the ratio between the two susceptibilities to $\chi_{xy}^A/\chi_{xy}^S = 0.5$, we simulate [25] the dichroic response $\Delta\bar{\Gamma}_{R-L}(\omega_{pp})$ under circular driving using two narrowband Gaussian fields of duration τ . The component $E_{\text{pu}}^y(\omega_s)$ is centered at frequency Ω , while $E_{\text{pu}}^x(\omega_s)$ is shifted by a small frequency mismatch $\Delta\Omega$.

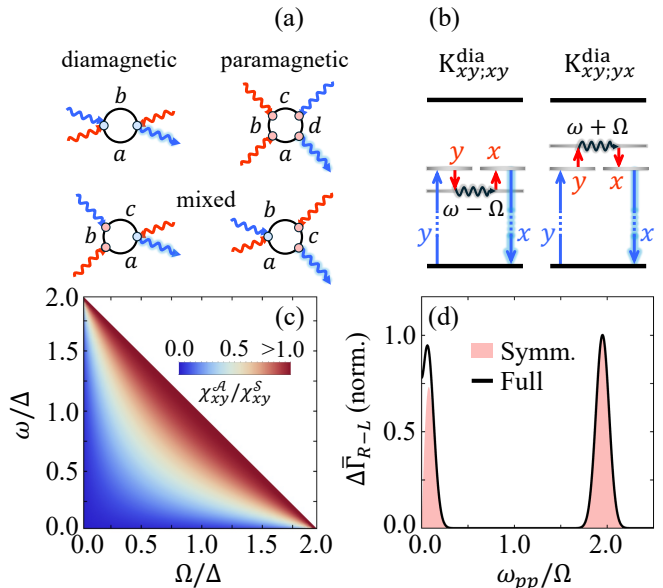


Figure 3. (a) Diagrammatic representation of the electronic processes contributing to the third-order susceptibility. Red (blue) wavy lines denote pump (probe) fields, while black lines represent electronic propagators. Red and blue dots denote velocity and density-like vertices, respectively. The probe photon on which the detection is performed is highlighted by a blue shadow. (b) Schematic representation of the two diamagnetic-like processes $K_{xy;xy}^{\text{dia}}$ and $K_{xy;yx}^{\text{dia}}$. Black (gray) lines denote real (virtual) electronic states. Red (blue) arrows represent pump (probe) fields. The intermediate state (black wavy line) propagates at frequencies $\omega \mp \Omega$, leading to distinct poles $d_{ab}(\omega \mp \Omega)$ and hence to a finite antisymmetric contribution K_{dia}^A , as in Eq. (9). (c) Map of the ratio χ_{xy}^A/χ_{xy}^S in the sp -model, for fixed $t/\Delta = 0.1$. The color scale is saturated for $\chi_{xy}^A/\chi_{xy}^S > 1$. (d) Dichroic response $\Delta\bar{\Gamma}_{R-L}$ for narrowband Gaussian pump pulses ($\Omega\tau = 20$) and frequency mismatch between E_{pu}^x and E_{pu}^y set to $\Delta\Omega/\Omega = 0.05$. The response is normalized to the 2Ω peak. The full response (black line) is obtained by fixing $\chi_{xy}^A/\chi_{xy}^S = 0.5$, while the red shaded area shows the symmetric contribution only.

The resulting spectrum is shown in Fig. 3(d) as a black line. For comparison, we also report as a red shaded area the response obtained by retaining only the symmetric contribution, corresponding to the Kleinman approximation $\chi_{xy}^A = 0$. In this case, the small but finite quasi-static signal associated with the light-induced Faraday effect is absent.

Although the quantitative results presented here are obtained within the sp -model, the many-body diagrammatic analysis is general. Therefore, while the overall magnitude of the light-induced Faraday response depends on material-specific details, the physical conclusions remain broadly applicable. For pump-probe conditions comparable to those realized in Ref. [9], namely $\omega/\Delta \simeq 1.65$ and $\Omega/\Delta \simeq 0.01$, our toy model with $t/\Delta = 0.1$ yields $\chi_{xy}^A/\chi_{xy}^S \simeq 0.1$, of the same order of magnitude as the value used in Fig. 3(d).

IV. PHONON CONTRIBUTION

In cubic SrTiO₃, the polar TO₁ phonon softens from 3.2 THz at 380 K to 1.8 THz at 150 K [30, 31]. As shown in Ref. [23], this softening naturally accounts for the pronounced temperature dependence of the Kerr response measured under linear driving: the ionic contribution is maximized at the temperature T_{res} at which the phonon is resonant with the pump frequency, and it is progressively suppressed away from it. Such a strong temperature dependence would be difficult to explain within a purely electronic picture, since a temperature variation of $\Delta T = 230$ K is expected to have only a negligible effect on the electronic response given the large direct band gap of SrTiO₃ ($2\Delta \simeq 3.75$ eV). A similar behavior is observed in Ref. [9] for the anomalous quasi-static signal measured under circular driving. Motivated by these observations, we now discuss the additional contribution of resonantly driven infrared-active phonons to the light-induced Faraday effect.

To describe the phonon-mediated response to circularly polarized light, we model the four-wave-mixing process as a phonon dressing of the antisymmetric electronic susceptibility, in which each pump photon excites an intermediate phonon state that subsequently recombines into off-resonant electronic excitations. This mechanism is represented diagrammatically in Fig. 4(a), and details of the derivation are provided in the Supplemental Material [25]. The dashed lines denote the phonon propagators

$$D(\Omega) = \frac{2\omega_0(T)}{\Omega^2 + 2i\gamma(T)\Omega - \omega_0^2(T)}, \quad (12)$$

where $\omega_0(T)$ and $\gamma(T)$ are the temperature-dependent phonon frequency and damping rate respectively. The vertex Z describes the linear light-phonon coupling, expressed in terms of paramagnetic and diamagnetic light-electron and electron-phonon couplings [32–34], and proportional to the Born effective charge Z_B of the mode as $Z = Z_B \sqrt{\omega_0(T)}/M$, with M the ionic mass [35]. The gray bubble represents the antisymmetric electronic susceptibility Π_{xy}^A , which includes diamagnetic, paramagnetic and mixed contributions analogous to those in Fig. 3(a), with electron-phonon vertices replacing the light-electron couplings on the pump side. The resulting antisymmetric optical susceptibility reads [25]

$$\chi_{xy}^{A,\text{ph}}(\omega; \omega, \Omega, -\Omega) = Z^2 D(\Omega) D(-\Omega) \times \Pi_{xy}^A(\omega; \omega, \Omega, -\Omega). \quad (13)$$

An analogous expression is found for the symmetric response [23]. The temperature dependence of this susceptibility is primarily governed by the phonon propagators Eq. (12), such that the phonon contribution to the light-induced Faraday effect is maximized at the temperature T_{res} satisfying the resonance condition $\Omega = \omega_0(T_{\text{res}})$, and is strongly suppressed away from it.

To illustrate the effect quantitatively, we compute the full response including both phonon-mediated and

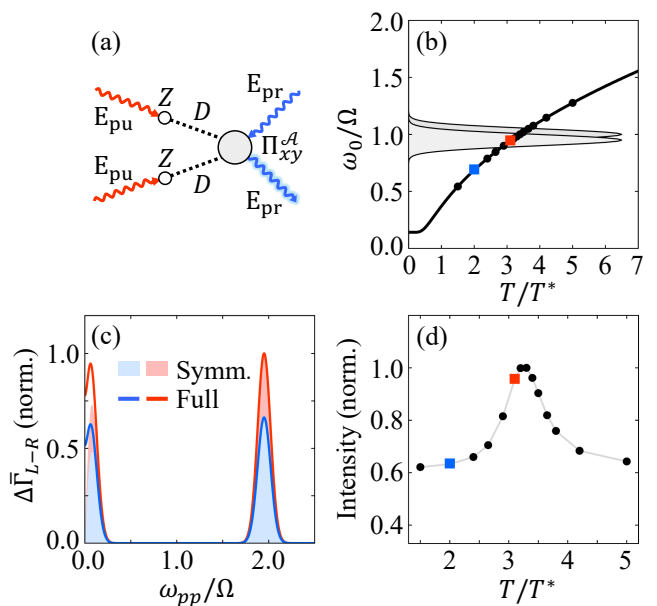


Figure 4. (a) Diagrammatic representation of the phonon-mediated contribution to the pump-probe response. Red (blue) wavy lines denote pump (probe) fields, and dashed black lines the phonon propagators. The linear light-phonon vertices Z are shown as white dots, while the gray bubble represents the electronic susceptibility Π_{xy}^A , including diamagnetic, paramagnetic, and mixed contributions. (b) Phenomenological temperature dependence of the phonon frequency $\omega_0(T)$ (black line), with $A/\Omega = 0.6$, $\omega_q/\Omega = 1.1$, and $T^*/\Omega = 1$. The phonon damping rate is $\gamma(T)/\omega_0(T) = 0.07$. Gray areas indicate the Gaussian pump field components E_{pu}^x and E_{pu}^y , with a relative frequency mismatch $\Delta\Omega/\Omega = 0.05$. Black dots and colored squares mark the temperatures analyzed in panels (c) and (d). (c) Dichroic signal including both electronic and phonon-mediated processes, evaluated at phonon resonance (red) and off resonance (blue), for the temperatures indicated in panel (b) with squares. Shaded areas show the symmetric contribution only, while solid lines include both the symmetric and the antisymmetric components. Calculations are performed for $\chi_{xy}^A/\chi_{xy}^S = \Pi_{xy}^A/\Pi_{xy}^S = 0.5$, and the relative weight between phonon-mediated and purely electronic processes is fixed by $\sqrt{\alpha}\beta Z_B/M = 0.06\Omega$. (d) Temperature dependence of the intensity of the light-induced Faraday response, for the selected temperatures of panel (b).

electronic processes. As discussed in the Supplemental Material [25], the relative weight between the two contributions can be expressed as $\chi_{xy}^{A,\text{ph}}/\chi_{xy}^A \sim \alpha(\beta Z_B/M)^2 D(\Omega)D(-\Omega)$, where β is a dimensionless parametrization of the electron-phonon coupling strength [34, 35], and α is a numerical constant of order one. The phonon softening is modeled as $\omega_0^2(T) = A(\omega_q \coth(\omega_q/T) - T^*)$, following the behavior of the TO₁ mode in SrTiO₃, with A , ω_q , and T^* treated as phenomenological parameters. We also assume a temperature-independent ratio $\gamma(T)/\omega_0(T)$ [30]. The temperature dependence of $\omega_0(T)$ is shown in Fig. 4(b),

together with the Gaussian narrowband pump components $E_{\text{pu}}^x(\omega_s)$ and $E_{\text{pu}}^y(\omega_s)$, shifted by a small frequency mismatch $\Delta\Omega$. In this parametrization, the phonon frequency crosses the pump spectrum within a finite temperature window, allowing a direct comparison between resonant and off-resonant conditions. In Fig. 4(c) we show the pump-probe response to circular light in both regimes. As expected, the signal is enhanced at resonance. Notably, however, the qualitative features of the response remain unchanged: in particular, the relative intensity of the quasi-static peak with respect to the 2Ω component is unaffected, as the phonon contributes equally to the symmetric and antisymmetric channels. In Fig. 4(d) we show the intensity of the light-induced Faraday response as a function of temperature, obtained by integrating the difference between the full response and its symmetric contribution over the pump-probe frequency ω_{pp} . This signal is maximized in the resonant regime, while remaining finite away from resonance due to the electronic contribution. This behavior is consistent with the experimental observations of Ref. [9], where a temperature window approximately corresponding to $2.5 \lesssim T/T^* \lesssim 3.8$ was investigated.

V. MAGNITUDE OF THE EFFECTIVE MAGNETIC FIELD

In the light-induced Faraday effect, a circularly polarized pump drives a rotation of the collective electronic polarization. Since this process does not involve macroscopic circulating currents, it does not generate a macroscopic magnetic field detectable outside the sample. Nevertheless, the resulting quasi-static rotation of the probe polarization can still be expressed in terms of an effective magnetic field that would induce the same rotation angle θ_F in the conventional direct Faraday effect. In the latter case, the Faraday rotation angle is proportional to the applied static magnetic field according to [2]

$$\theta_F = \xi \chi^{(F)} H^z = V l_{\text{eff}} H^z. \quad (14)$$

Here $\xi = \pi l_{\text{eff}}/n_{\text{pr}}\lambda_{\text{pr}}$, where l_{eff} is the effective interaction length and n_{pr} the refractive index at the probe wavelength λ_{pr} , while $V = \pi\chi^{(F)}/n_{\text{pr}}\lambda_{\text{pr}}$ denotes the Verdet constant of the material. Frequency dependence is kept implicit for compactness. In the light-induced Faraday effect the quasi-static probe rotation instead originates from the antisymmetric nonlinear susceptibility. Comparing Eqs. (1) and (2), one can identify the combination $\chi^{(F)} H^z$ of the conventional Faraday effect with $\chi_{xy}^A (|\mathcal{E}_L|^2 - |\mathcal{E}_R|^2)$, which reduces to $\chi_{xy}^A |\mathcal{E}_{\text{pu}}|^2$ for a purely left- or right-circularly polarized light. As a consequence, the static probe rotation induced by a monochromatic pump can be written in direct analogy with Eq. (14) as

$$\theta_{\text{LIF}} = \xi \chi_{xy}^A |\mathcal{E}_{\text{pu}}|^2. \quad (15)$$

For a rough quantitative estimate, we consider SrTiO₃ at room temperature using the experimental parameters

of Ref. [9]. In particular, one has $l_{\text{eff}} = 2.49 \mu\text{m}$ and $n_{\text{pr}} = 2.6$ for a $\lambda_{\text{pr}} = 400 \text{ nm}$ probe. We then take the static value for the symmetric susceptibility $\chi_{xy}^S = 10^{-10} \text{ cm}^2/\text{kV}^2$ [36], and fix the ratio $\chi_{xy}^A/\chi_{xy}^S = 0.5$ to reproduce the experimentally observed relative magnitude between Kerr and light-induced Faraday responses. For a pump field strength $|\mathcal{E}_{\text{pu}}| = 230 \text{ kV/cm}$, Eq. (15) yields a rotation angle $\theta_{\text{LIF}} \simeq 20 \mu\text{rad}$, consistent with the measured values.

The corresponding effective magnetic field can then be estimated from Eq. (14) using $V \simeq 250 \text{ rad/m} \cdot \text{T}$, obtaining

$$H_{\text{eff}} = \theta_{\text{LIF}}/V l_{\text{eff}} \simeq 30 \text{ mT}. \quad (16)$$

Although this corresponds to a remarkably large field, it is not connected to the emergence of an anomalous macroscopic magnetization. Instead, it represents the effective field associated with the dynamical nonlinear optical response, and it cannot be detected outside the material [20, 21].

VI. CONCLUSION

In this work we developed a microscopic theory of the dynamical breaking of time-reversal symmetry in solids driven by circularly polarized light, identifying the resulting nonlinear response as a light-induced Faraday effect. We showed that a static probe rotation originates from the antisymmetric component of the third-order susceptibility, and demonstrated that such a contribution emerges only in dynamical conditions as a consequence of the breakdown of Kleinman symmetry, yielding sizeable effects even far from dissipative resonances. The light-induced Faraday effect can thus be interpreted as the optical analogue of a Faraday rotation generated by an effective internal magnetic field associated with the pump-driven electronic excitations, despite the absence of any real macroscopic magnetization.

To establish a quantitative connection with the recent experiments on paraelectric SrTiO₃ [9], several additional effects must be taken into account. A crucial aspect is that, under realistic pump conditions, the two components of the circular field may exhibit a small frequency mismatch. In such cases, the symmetric susceptibility also contributes to the quasi-static response through a Kerr-like component, which can often provide the dominant signal. Since this symmetric term remains finite in the static approximation, it could already be captured in previous modeling [9, 23]. Neglecting this symmetric contribution, however, can lead to an overestimate of the anomalous response in attempts to explain the full signal [15, 16, 20, 21]. At the same time, we find that the additional residual quasi-static signal reported in Ref. [9] is compatible with the light-induced Faraday response predicted here for SrTiO₃ under comparable experimental conditions. Furthermore, by including

the phonon-mediated contribution to the susceptibility, strongly modulated by the softening of the polar mode, our framework also reproduces the pronounced temperature dependence observed experimentally, in analogy with the behavior previously identified for the Kerr response under linearly polarized driving [23]. Altogether, these results suggest that the quasi-static signal observed in Ref. [9] can be naturally interpreted within a light-induced Faraday scenario, without the need to invoke anomalously large phononic magnetic moments [11–14].

We note that a fully quantitative match between theory and experiment would require evaluating the dynamical nonlinear response using the realistic band structure of the material, alongside a careful treatment of propagation and phase-matching effects. These are known to introduce nontrivial features in THz pump-visible probe experiments, where the fields propagate with considerably different phase velocities [37–40].

As discussed, the probe rotation induced by the light-induced Faraday effect can be associated with a fictitious magnetic field reaching strengths on the order of tens of mT with a THz pump. In principle, this effective field could be further amplified by increasing the pump

frequency, owing to the corresponding enhancement of the antisymmetric susceptibility. Beyond its immediate relevance for interpreting recent ultrafast experiments, our results open a broader perspective on the possibility of engineering tunable nonequilibrium dichroic optical devices, and potentially realizing magneto-optical and transport phenomena in otherwise nonmagnetic materials.

ACKNOWLEDGMENTS

We are grateful to Roberto Merlin, Martina Basini, and Mattia Udina for useful discussions and suggestions. This work has been supported by the European Union under the project MORE-TEM ERC-SYN (Grant No. 951215); by Sapienza University under the project Ateneo (Grants No. RM123188E357C540, and No. RP124190A63FAA97); and by the Italian Ministry of Education, University and Research under Project PRIN2022-CoInEx (Grant No. 2022WS9MS4).

-
- [1] P. S. Pershan, Phys. Rev. **130**, 919 (1963).
 - [2] J. P. van der Ziel, P. S. Pershan, and L. D. Malmstrom, Phys. Rev. Lett. **15**, 190 (1965).
 - [3] P. S. Pershan, J. P. van der Ziel, and L. D. Malmstrom, Phys. Rev. **143**, 574 (1966).
 - [4] A. Kimel, A. Kirilyuk, P. Usachev, R. Pisarev, A. Balbashov, and T. Rasing, Nature **435**, 655 (2005).
 - [5] M. J. Freiser, IEEE Transactions on Magnetics **4**, 152 (1968).
 - [6] G. R. Fowles and D. W. Lynch, American Journal of Physics **36**, 770 (1968).
 - [7] A. Kirilyuk, A. V. Kimel, and T. Rasing, Rev. Mod. Phys. **82**, 2731 (2010).
 - [8] R. V. Mikhaylovskiy, E. Hendry, and V. V. Kruglyak, Phys. Rev. B **86**, 100405 (2012).
 - [9] M. Basini, M. Pancaldi, B. Wehinger, M. Udina, V. Unikandanunni, T. Tadano, M. C. Hoffmann, A. V. Balatsky, and S. Bonetti, Nature **628**, 534 (2024).
 - [10] C. Davies, F. Fennema, A. Tsukamoto, I. Razdolski, A. Kimel, and A. Kirilyuk, Nature **628**, 540 (2024).
 - [11] D. M. Juraschek, M. Fechner, A. V. Balatsky, and N. A. Spaldin, Phys. Rev. Mater. **1**, 014401 (2017).
 - [12] D. M. Juraschek and N. A. Spaldin, Phys. Rev. Mater. **3**, 064405 (2019).
 - [13] D. M. Juraschek, P. Narang, and N. A. Spaldin, Phys. Rev. Res. **2**, 043035 (2020).
 - [14] D. M. Juraschek, T. c. v. Neuman, and P. Narang, Phys. Rev. Res. **4**, 013129 (2022).
 - [15] N. Shabala and R. M. Geilhufe, Phys. Rev. Lett. **133**, 266702 (2024).
 - [16] L. Klebl, A. Schobert, M. Eckstein, G. Sangiovanni, A. V. Balatsky, and T. O. Wehling, Phys. Rev. Lett. **134**, 016705 (2025).
 - [17] C. P. Romao and D. M. Juraschek, Nature **628**, 505 (2024).
 - [18] D. A. B. Lopez, W. Hu, and D. M. Juraschek, Phys. Rev. B **112**, 144306 (2025).
 - [19] H. Chen, W. Chen, K. Yang, T. Cao, and D. Xiao, “Nonadiabatic theory of phonon magnetic moments in insulators and metals,” (2026), arXiv:2605.06983 [cond-mat.mes-hall].
 - [20] R. Merlin, Phys. Rev. B **110**, 094312 (2024).
 - [21] R. Merlin, PNAS Nexus **4**, pgaf002 (2025).
 - [22] R. W. Boyd, in *Nonlinear Optics (Fourth Edition)* (Academic Press, 2020) fourth edition ed., pp. 1–64.
 - [23] M. Basini, M. Udina, M. Pancaldi, V. Unikandanunni, S. Bonetti, and L. Benfatto, Phys. Rev. B **109**, 024309 (2024).
 - [24] E. Jiménez, N. Mikuszeit, J. L. F. Cuñado, P. Perna, J. Pedrosa, D. Maccariello, C. Rodrigo, M. A. Niño, A. Bollero, J. Camarero, and R. Miranda, Review of Scientific Instruments **85**, 053904 (2014).
 - [25] See Supplemental Information for the derivation of the differential intensity at generic sample orientation for linearly and circularly polarized monochromatic light; the derivation of the differential intensity for frequency-mismatched monochromatic and Gaussian pumps; details of the calculations of the antisymmetric kernel in the *sp* model; and details of the calculations of the phonon-mediated response.
 - [26] J. Fiore, N. Sellati, M. Udina, and L. Benfatto, Phys. Rev. B **113**, 174524 (2026).
 - [27] L. Benfatto, A. Toschi, and S. Caprara, Phys. Rev. B **69**, 184510 (2004).
 - [28] M. Udina, T. Cea, and L. Benfatto, Phys. Rev. B **100**, 165131 (2019).
 - [29] M. Udina and I. Paul, Phys. Rev. Lett. **136**, 126505 (2026).

- [30] H. Vogt, Phys. Rev. B **51**, 8046 (1995).
- [31] Y. Yamada and G. Shirane, Journal of the Physical Society of Japan **26**, 396 (1969), <https://doi.org/10.1143/JPSJ.26.396>.
- [32] E. Cappelluti, L. Benfatto, and A. B. Kuzmenko, Phys. Rev. B **82**, 041402 (2010).
- [33] E. Cappelluti, L. Benfatto, M. Manzardo, and A. B. Kuzmenko, Phys. Rev. B **86**, 115439 (2012).
- [34] O. Bistoni, P. Barone, E. Cappelluti, L. Benfatto, and F. Mauri, 2D Materials **6**, 045015 (2019).
- [35] R. Resta, Rev. Mod. Phys. **66**, 899 (1994).
- [36] Y. Deng, Y. Du, M. Zhang, J. Han, and Z. Yin, Solid State Communications **135**, 221 (2005).
- [37] L. Huber, S. F. Maehrlein, F. Wang, Y. Liu, and X.-Y. Zhu, The Journal of Chemical Physics **154**, 094202 (2021).
- [38] S. F. Maehrlein, P. P. Joshi, L. Huber, F. Wang, M. Cherasse, Y. Liu, D. M. Juraschek, E. Mosconi, D. Meggiolaro, F. D. Angelis, and X.-Y. Zhu, Proceedings of the National Academy of Sciences **118**, e2022268118 (2021).
- [39] M. Frenzel, M. Cherasse, J. M. Urban, F. Wang, B. Xiang, L. Nest, L. Huber, L. Perfetti, M. Wolf, T. Kampfrath, X.-Y. Zhu, and S. F. Maehrlein, Science Advances **9**, eadg3856 (2023).
- [40] N. Sellati, J. Fiore, S. P. Villani, L. Benfatto, and M. Udina, npj Quantum Materials **10**, 46 (2025).

Dynamical time-reversal symmetry breaking from Kleinman symmetry breakdown - Supplemental Material

Niccolò Sellati¹, Jacopo Fiore^{1,2}, Lara Benfatto¹

¹*Department of Physics, "Sapienza" University of Rome, P.le A. Moro 5, 00185 Rome, Italy*

²*Institute for Theory of Statistical Physics, RWTH Aachen University, Aachen, Germany*

CALCULATION OF THE DIFFERENTIAL INTENSITY

In the balanced detection scheme as the one reported in Refs. [9, 23], the differential intensity $\Delta\Gamma$ is directly proportional to the nonlinear polarization induced in the direction P , orthogonal to the polarization of the incoming probe along the direction S . Following the geometry described in Fig. 1(b) of the main text, reported here in Fig. S1, $\Delta\Gamma$ can then be connected to the nonlinear polarizations induced along the crystallographic x and y directions as

$$\Delta\Gamma \propto P_{\text{NL}}^P = \cos\theta P_{\text{NL}}^x - \sin\theta P_{\text{NL}}^y. \quad (\text{S1})$$

The results reported in the main text are obtained from the following calculations by setting $\theta = 0$. Along the i -th direction ($i = x, y$), we can link the third-order nonlinear polarization P_{NL}^i to the external electric field through the rank-4 third-order nonlinear susceptibility $\chi_{ijkl}(\omega; \omega_1, \omega_2, \omega_3)$. For the experimental geometry considered, we have explicitly

$$P_{\text{NL}}^i(\omega) = \sum_{j,k,l=x,y} \int d\omega_1 d\omega_2 d\omega_3 \delta(\omega - \omega_1 - \omega_2 - \omega_3) \chi_{ijkl}(\omega; \omega_1, \omega_2, \omega_3) E^j(\omega_1) E^k(\omega_2) E^l(\omega_3). \quad (\text{S2})$$

We then introduce the time delay t_{pp} between pump \mathbf{E}_{pu} and probe \mathbf{E}_{pr} , such that the total applied electric field is $\mathbf{E}(t, t_{pp}) = \mathbf{E}_{\text{pu}}(t + t_{pp}) + \mathbf{E}_{\text{pr}}(t)$. For a single s component, and by taking the Fourier transform with respect to t , this is equivalent to substituting

$$E^s(\omega_s) \rightarrow E^s(\omega_s, t_{pp}) = E_{\text{pr}}^s(\omega_s) + E_{\text{pu}}^s(\omega_s) e^{-i\omega_s t_{pp}}, \quad (\text{S3})$$

and thus rewrite Eq. (S2) as

$$P_{\text{NL}}^i(\omega, t_{pp}) = 3 \sum_{j,k,l=x,y} \int d\omega_1 d\omega_2 d\omega_3 \delta(\omega - \omega_1 - \omega_2 - \omega_3) \chi_{ij;kl}(\omega; \omega_1, \omega_2, \omega_3) E_{\text{pr}}^j(\omega_1) E_{\text{pu}}^k(\omega_2) E_{\text{pu}}^l(\omega_3) e^{-i(\omega_2 + \omega_3)t_{pp}}. \quad (\text{S4})$$

Here we retained only terms scaling in $E_{\text{pr}} E_{\text{pu}}^2$, relevant for the pump-probe experiment. The third order susceptibility $\chi_{ij;kl}$ with the semicolon implies a precise ordering of the Cartesian indices, with i labeling the outgoing nonlinear signal, j the incoming probe, k and l the pump fields.

In the following we consider a cubic crystal with four independent components of the susceptibility, $\chi_{ii;ii}(\omega; \omega_1, \omega_2, \omega_3)$, $\chi_{ii;jj}(\omega; \omega_1, \omega_2, \omega_3)$, $\chi_{ij;ij}(\omega; \omega_1, \omega_2, \omega_3)$ and $\chi_{ij;ji}(\omega; \omega_1, \omega_3, \omega_2)$ ($i, j = x, y$ and $i \neq j$), and separate $P_{\text{NL}}^i(\omega, t_{pp})$ into three contributions:

$$P_{\text{NL}}^i(\omega, t_{pp}) = 3 \int d\omega_1 d\omega_2 d\omega_3 \delta(\omega - \omega_1 - \omega_2 - \omega_3) e^{-i(\omega_2 + \omega_3)t_{pp}} \left[\begin{aligned} &\chi_{ii;ii}(\omega; \omega_1, \omega_2, \omega_3) E_{\text{pr}}^i(\omega_1) E_{\text{pu}}^i(\omega_2) E_{\text{pu}}^i(\omega_3) \\ &\chi_{ii;jj}(\omega; \omega_1, \omega_2, \omega_3) E_{\text{pr}}^i(\omega_1) E_{\text{pu}}^j(\omega_2) E_{\text{pu}}^j(\omega_3) \\ &(\chi_{ij;ij}(\omega; \omega_1, \omega_2, \omega_3) + \chi_{ij;ji}(\omega; \omega_1, \omega_3, \omega_2)) E_{\text{pr}}^j(\omega_1) E_{\text{pu}}^i(\omega_2) E_{\text{pu}}^j(\omega_3) \end{aligned} \right]. \quad (\text{S5})$$

If the xy crystallographic reference frame is rotated with respect to the PS reference frame in the experiment, it is more convenient to express the fields with their P and S components, as

$$\begin{aligned} E_{\text{pr}}^x &= E_{\text{pr}}^S \sin\theta = E_{\text{pr}} \sin\theta, \\ E_{\text{pr}}^y &= E_{\text{pr}}^S \cos\theta = E_{\text{pr}} \cos\theta, \end{aligned} \quad (\text{S6})$$

and

$$\begin{aligned} E_{\text{pu}}^x &= E_{\text{pu}}^S \sin(\theta + \Delta\theta) + E_{\text{pu}}^P \cos(\theta + \Delta\theta), \\ E_{\text{pu}}^y &= E_{\text{pu}}^S \cos(\theta + \Delta\theta) - E_{\text{pu}}^P \sin(\theta + \Delta\theta). \end{aligned} \quad (\text{S7})$$

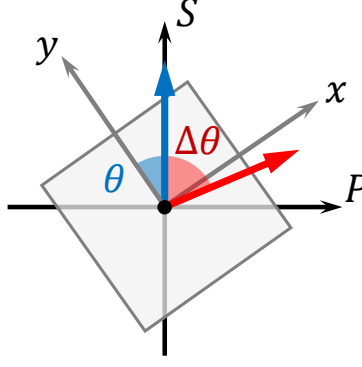


Figure S1. Polarization geometry. The probe (blue) defines a fixed PS reference frame, while the sample is rotated by an angle θ . The pump (red) is described in a reference frame rotated by a fixed angle $\Delta\theta$ with respect to PS .

Here, $\Delta\theta$ is the angle between the pump polarization at $t_{pp} = 0$ and the PS reference frame (see Fig. S1). We note that this angle is fixed in the experiment.

Finally, using Eq. (S5) with the rotations Eqs. (S6) and (S7), we can rewrite the differential signal Eq. (S1) as

$$\Delta\Gamma(t_{pp}, \theta) \propto \int d\omega_1 d\omega_2 d\omega_3 e^{-i(\omega_2 + \omega_3)t_{pp}} E_{\text{pr}}(\omega_1) \left[(F_{23}(\theta) + F_{32}(\theta))\mathcal{S}_{\parallel} + (G_{23}(\theta) + G_{32}(\theta))\mathcal{S}_{\perp} + (H_{23} - H_{32})\mathcal{A} \right], \quad (\text{S8})$$

where we performed an integration over ω , as dictated by the detection procedure of pump-probe experiments [28], and $\int d\omega \delta(\omega - \omega_1 - \omega_2 - \omega_3) = 1$. As defined in Eq. (5) of the main text, $\mathcal{S}_{\parallel, \perp}$ and \mathcal{A} denote, respectively, symmetric and antisymmetric combinations of the pump field components under exchange $\omega_2 \leftrightarrow \omega_3$,

$$\begin{aligned} \mathcal{S}_{\parallel} &= E_{\text{pu}}^S(\omega_2)E_{\text{pu}}^S(\omega_3) - E_{\text{pu}}^P(\omega_2)E_{\text{pu}}^P(\omega_3), \\ \mathcal{S}_{\perp} &= E_{\text{pu}}^P(\omega_2)E_{\text{pu}}^S(\omega_3) + E_{\text{pu}}^S(\omega_2)E_{\text{pu}}^P(\omega_3), \\ \mathcal{A} &= E_{\text{pu}}^P(\omega_2)E_{\text{pu}}^S(\omega_3) - E_{\text{pu}}^S(\omega_2)E_{\text{pu}}^P(\omega_3), \end{aligned} \quad (\text{S9})$$

where the subscripts \parallel and \perp indicate that each product contain parallel or perpendicular components of the pump field. The coefficients of the symmetric combinations read explicitly

$$\begin{aligned} F_{kl}(\theta) &= \frac{1}{2} \left[\frac{\sin(4\theta) \cos(2\Delta\theta)}{2} (\chi_{ii;jj}(\omega; \omega_1, \omega_k, \omega_l) + \chi_{ij;jj}(\omega; \omega_1, \omega_k, \omega_l) + \chi_{ij;ji}(\omega; \omega_1, \omega_l, \omega_k) - \chi_{ii;ii}(\omega; \omega_1, \omega_k, \omega_l)) \right. \\ &\quad + \sin^2(2\theta) \sin(2\Delta\theta) (\chi_{ii;ii}(\omega; \omega_1, \omega_k, \omega_l) - \chi_{ii;jj}(\omega; \omega_1, \omega_k, \omega_l) - \chi_{ij;jj}(\omega; \omega_1, \omega_k, \omega_l) - \chi_{ij;ji}(\omega; \omega_1, \omega_l, \omega_k)) \\ &\quad \left. + \sin(2\Delta\theta) (\chi_{ij;ij}(\omega; \omega_1, \omega_k, \omega_l) + \chi_{ij;ji}(\omega; \omega_1, \omega_l, \omega_k)) \right] \equiv F(\omega_1, \omega_k, \omega_l, \theta) \equiv F_{\omega_k \omega_l}(\theta), \end{aligned} \quad (\text{S10})$$

and

$$\begin{aligned} G_{kl}(\theta) &= \frac{1}{2} \left[\frac{\sin(4\theta) \sin(2\Delta\theta)}{2} (\chi_{ii;jj}(\omega; \omega_1, \omega_k, \omega_l) + \chi_{ij;jj}(\omega; \omega_1, \omega_k, \omega_l) + \chi_{ij;ji}(\omega; \omega_1, \omega_l, \omega_k) - \chi_{ii;ii}(\omega; \omega_1, \omega_k, \omega_l)) \right. \\ &\quad + \sin^2(2\theta) \cos(2\Delta\theta) (\chi_{ii;ii}(\omega; \omega_1, \omega_k, \omega_l) - \chi_{ii;jj}(\omega; \omega_1, \omega_k, \omega_l) - \chi_{ij;jj}(\omega; \omega_1, \omega_k, \omega_l) - \chi_{ij;ji}(\omega; \omega_1, \omega_l, \omega_k)) \\ &\quad \left. + \cos(2\Delta\theta) (\chi_{ij;ij}(\omega; \omega_1, \omega_k, \omega_l) + \chi_{ij;ji}(\omega; \omega_1, \omega_l, \omega_k)) \right] \equiv G(\omega_1, \omega_k, \omega_l, \theta) \equiv G_{\omega_k \omega_l}(\theta). \end{aligned} \quad (\text{S11})$$

Notice that when the combinations $F_{23}(\theta) + F_{32}(\theta)$ and $G_{23}(\theta) + G_{32}(\theta)$ are taken in Eq. (S8), $\chi_{ij;jj}$ and $\chi_{ij;ji}$ only appear through their symmetric combination,

$$\chi_{ij}^S(\omega; \omega_1, \omega_2, \omega_3) = \chi_{ij;jj}(\omega; \omega_1, \omega_2, \omega_3) + \chi_{ij;ji}(\omega; \omega_1, \omega_2, \omega_3). \quad (\text{S12})$$

Moreover, for $\theta = 0$ or $\theta = \pi/2$, i.e., with a probe aligned with one of the crystallographic axes, terms scaling with $\chi_{ii;ii}$ and $\chi_{ii;jj}$ vanish, leaving only the response mediated by χ_{ij}^S , as it is considered in the main text.

The coefficient of the antisymmetric combination, on the other hand, reads explicitly

$$H_{kl} = H(\omega_1, \omega_k, \omega_l) = \frac{1}{2}(\chi_{ij;ij}(\omega; \omega_1, \omega_k, \omega_l) + \chi_{ij;ji}(\omega; \omega_1, \omega_l, \omega_k)) = \chi_{ij;ij}(\omega; \omega_1, \omega_k, \omega_l), \quad (\text{S13})$$

with no dependence on the angle θ . The combination appearing in Eq. (S8) can then be rewritten immediately as

$$H_{23} - H_{32} = \chi_{ij;ij}(\omega; \omega_1, \omega_2, \omega_3) - \chi_{ij;ij}(\omega; \omega_1, \omega_3, \omega_2), \quad (\text{S14})$$

which is explicitly antisymmetric under the exchange $\omega_2 \leftrightarrow \omega_3$. Using $\chi_{ij;ij}(\omega; \omega_1, \omega_3, \omega_2) = \chi_{ij;ji}(\omega; \omega_1, \omega_2, \omega_3)$, such frequency antisymmetry can be equivalently recast as an antisymmetry under the exchange of the Cartesian pump indices, leading to

$$H_{23} - H_{32} = \chi_{ij}^A(\omega; \omega_1, \omega_2, \omega_3) = \chi_{ij;ij}(\omega; \omega_1, \omega_2, \omega_3) - \chi_{ij;ji}(\omega; \omega_1, \omega_2, \omega_3). \quad (\text{S15})$$

Both Eqs. (S14) and (S15) make it evident that the antisymmetric response is lost when Kleinman symmetry is enforced, corresponding to taking the static limit of the susceptibility in which $\chi_{ij;ij}(0; 0, 0, 0) = \chi_{ij;ji}(0; 0, 0, 0)$.

Eq. (S8) represents the differential intensity $\Delta\Gamma(t_{pp}, \theta)$ measured for generic spectral content of the pump and probe fields, and for a generic polarization of the pump. We note that this expression assumes that all possible generated harmonics of the probe are collected by the photodetectors. A realistic detection setup has a limited spectral range, which can be taken into account with an appropriate function $R(\omega)$ when performing the integral over ω .

PUMP-PROBE SIGNAL UNDER MONOCHROMATIC PUMP PULSES

To further analyze the spectral response of the pump-probe experiment, we consider monochromatic fields at frequency Ω ,

$$\begin{aligned} E_{\text{pu}}^P(\omega_s) &= \mathcal{E}_P \delta(\omega_s - \Omega) + \mathcal{E}_P^* \delta(\omega_s + \Omega), \\ E_{\text{pu}}^S(\omega_s) &= \mathcal{E}_S \delta(\omega_s - \Omega) + \mathcal{E}_S^* \delta(\omega_s + \Omega), \end{aligned} \quad (\text{S16})$$

where $\mathcal{E}_{P,S}$ are the complex field amplitudes. By using Eq. (S16) in Eq. (S9), we then find

$$\begin{aligned} \mathcal{S}_{\parallel} &= (\mathcal{E}_S^2 - \mathcal{E}_P^2) \delta(\omega_2 - \Omega) \delta(\omega_3 - \Omega) + (\mathcal{E}_S^{*2} - \mathcal{E}_P^{*2}) \delta(\omega_2 + \Omega) \delta(\omega_3 + \Omega) \\ &\quad + (|\mathcal{E}_S|^2 - |\mathcal{E}_P|^2) (\delta(\omega_2 - \Omega) \delta(\omega_3 + \Omega) + \delta(\omega_2 + \Omega) \delta(\omega_3 - \Omega)), \end{aligned} \quad (\text{S17})$$

and

$$\begin{aligned} \mathcal{S}_{\perp} &= 2\mathcal{E}_P \mathcal{E}_S \delta(\omega_2 - \Omega) \delta(\omega_3 - \Omega) + 2\mathcal{E}_P^* \mathcal{E}_S^* \delta(\omega_2 + \Omega) \delta(\omega_3 + \Omega) \\ &\quad + (\mathcal{E}_P \mathcal{E}_S^* + \mathcal{E}_P^* \mathcal{E}_S) (\delta(\omega_2 - \Omega) \delta(\omega_3 + \Omega) + \delta(\omega_2 + \Omega) \delta(\omega_3 - \Omega)), \end{aligned} \quad (\text{S18})$$

for the symmetric combinations of the fields, and

$$\mathcal{A} = (\mathcal{E} \times \mathcal{E}^*)_z (\delta(\omega_2 - \Omega) \delta(\omega_3 + \Omega) - \delta(\omega_2 + \Omega) \delta(\omega_3 - \Omega)), \quad (\text{S19})$$

for the antisymmetric combination. Here, $\mathcal{E} = (\mathcal{E}_P, \mathcal{E}_S)$, and $(\mathcal{E} \times \mathcal{E}^*)_z = \mathcal{E}_P \mathcal{E}_S^* - \mathcal{E}_P^* \mathcal{E}_S$.

Linearly polarized light

For linearly polarized light, the P and S components of the electric field are in phase, such that $\mathcal{E}_P \mathcal{E}_S^* = \mathcal{E}_P^* \mathcal{E}_S$. As a consequence, the cross product $\mathcal{E} \times \mathcal{E}^*$ vanishes, and the antisymmetric contribution is identically zero. Using Eqs. (S17) and (S18) into the differential signal $\Delta\Gamma(t_{pp}, \theta)$ in Eq. (S8) one obtains the response to linearly polarized pump pulses, which exhibits oscillations at $\omega_2 + \omega_3 = \pm 2\Omega$ and $\omega_2 + \omega_3 = 0$. In Fourier space, $\Delta\Gamma(t_{pp}, \theta) \rightarrow \Delta\bar{\Gamma}(\omega_{pp}, \theta)$, we find for the three spectral components

$$\Delta\bar{\Gamma}(2\Omega, \theta) \propto 2 \int d\omega_1 E_{\text{pr}}(\omega_1) \left[F_{\Omega\Omega}(\theta) (\mathcal{E}_S^2 - \mathcal{E}_P^2) + 2G_{\Omega\Omega}(\theta) \mathcal{E}_P \mathcal{E}_S \right], \quad (\text{S20})$$

$$\Delta\bar{\Gamma}(-2\Omega, \theta) \propto 2 \int d\omega_1 E_{\text{pr}}(\omega_1) \left[F_{-\Omega-\Omega}(\theta) (\mathcal{E}_S^{*2} - \mathcal{E}_P^{*2}) + 2G_{-\Omega-\Omega}(\theta) \mathcal{E}_P^* \mathcal{E}_S^* \right], \quad (\text{S21})$$

$$\Delta\bar{\Gamma}(0, \theta) \propto 2 \int d\omega_1 E_{\text{pr}}(\omega_1) \left[(F_{\Omega-\Omega}(\theta) + F_{-\Omega\Omega}(\theta)) (|\mathcal{E}_S|^2 - |\mathcal{E}_P|^2) + (G_{\Omega-\Omega}(\theta) + G_{-\Omega\Omega}(\theta)) (\mathcal{E}_P \mathcal{E}_S^* + \mathcal{E}_P^* \mathcal{E}_S) \right]. \quad (\text{S22})$$

Because only the symmetric combinations contribute to the pump-probe signal, the same result could be obtained enforcing Kleinman symmetry, as it was done in Ref. [23]. Also we note that all spectral components of the signal have fourfold angular dependence, coming directly from $F_{kl}(\theta)$ and $G_{kl}(\theta)$ in Eqs. (S10) and (S11) [23].

Circularly polarized light

For circularly polarized light it is convenient to recast the complex field amplitudes $\mathcal{E}_{P,S}$ in the circular basis $\mathcal{E}_{L,R}$ as

$$\begin{aligned} \mathcal{E}_L &= \frac{1}{\sqrt{2}} (\mathcal{E}_P + i\mathcal{E}_S), \\ \mathcal{E}_R &= \frac{1}{\sqrt{2}} (\mathcal{E}_P - i\mathcal{E}_S). \end{aligned} \quad (\text{S23})$$

With such a change of variables, we can rewrite Eqs. (S17), (S18) and (S19) as

$$\begin{aligned} \mathcal{S}_{\parallel} = & - (\mathcal{E}_L^2 + \mathcal{E}_R^2) \delta(\omega_2 - \Omega) \delta(\omega_3 - \Omega) - (\mathcal{E}_L^{*2} + \mathcal{E}_R^{*2}) \delta(\omega_2 + \Omega) \delta(\omega_3 + \Omega) \\ & - (\mathcal{E}_L \mathcal{E}_R^* + \mathcal{E}_L^* \mathcal{E}_R) (\delta(\omega_2 - \Omega) \delta(\omega_3 + \Omega) + \delta(\omega_2 + \Omega) \delta(\omega_3 - \Omega)), \end{aligned} \quad (\text{S24})$$

$$\begin{aligned} \mathcal{S}_{\perp} = & - i(\mathcal{E}_L^2 - \mathcal{E}_R^2) \delta(\omega_2 - \Omega) \delta(\omega_3 - \Omega) + i(\mathcal{E}_L^{*2} - \mathcal{E}_R^{*2}) \delta(\omega_2 + \Omega) \delta(\omega_3 + \Omega) \\ & - i(\mathcal{E}_L \mathcal{E}_R^* - \mathcal{E}_L^* \mathcal{E}_R) (\delta(\omega_2 - \Omega) \delta(\omega_3 + \Omega) + \delta(\omega_2 + \Omega) \delta(\omega_3 - \Omega)), \end{aligned} \quad (\text{S25})$$

and

$$\mathcal{A} = i(|\mathcal{E}_L|^2 - |\mathcal{E}_R|^2) (\delta(\omega_2 - \Omega) \delta(\omega_3 + \Omega) - \delta(\omega_2 + \Omega) \delta(\omega_3 - \Omega)). \quad (\text{S26})$$

In the following and in the main text we neglect terms in $\mathcal{E}_L \mathcal{E}_R^*$ or $\mathcal{E}_L^* \mathcal{E}_R$, considering an experiment performed either with purely left-handed or right-handed circular light. As a consequence, one can immediately see that the symmetric terms only contribute to the response in $\pm 2\Omega$, while the antisymmetric one only contributes to the static response. Using Eqs. (S24), (S25) and (S26) in Eq. (S8), one explicitly finds for the three spectral components

$$\Delta\bar{\Gamma}(2\Omega, \theta) \propto -2 \int d\omega_1 \mathbf{E}_{\text{pr}}(\omega_1) \left[F_{\Omega\Omega}(\theta) (\mathcal{E}_L^2 + \mathcal{E}_R^2) + iG_{\Omega\Omega}(\theta) (\mathcal{E}_L^2 - \mathcal{E}_R^2) \right], \quad (\text{S27})$$

which reduces to Eq. (7) of the main text for $\theta = 0$ and monochromatic probe field $\mathbf{E}_{\text{pr}}(\omega_1) \propto \delta(\omega_1 - \omega) + \delta(\omega_1 + \omega)$,

$$\Delta\bar{\Gamma}(-2\Omega, \theta) \propto -2 \int d\omega_1 \mathbf{E}_{\text{pr}}(\omega_1) \left[F_{-\Omega-\Omega}(\theta) (\mathcal{E}_L^{*2} + \mathcal{E}_R^{*2}) - iG_{-\Omega-\Omega}(\theta) (\mathcal{E}_L^{*2} - \mathcal{E}_R^{*2}) \right], \quad (\text{S28})$$

and

$$\Delta\bar{\Gamma}(0) \propto 2 \int d\omega_1 \mathbf{E}_{\text{pr}}(\omega_1) \left[i\chi_{ij}^A(\omega; \omega_1, \Omega, -\Omega) (|\mathcal{E}_L|^2 - |\mathcal{E}_R|^2) \right], \quad (\text{S29})$$

which corresponds to Eq. (8) of the main text for monochromatic probe. We note that the whole static response does not display any angular dependence, as it is given only by the antisymmetric term. Contributions scaling with $\mathcal{E}_L^2 + \mathcal{E}_R^2$ and $\mathcal{E}_L^{*2} + \mathcal{E}_R^{*2}$ are canceled in the dichroic signal $\Delta\bar{\Gamma}_{R-L} = \frac{1}{2}(\Delta\bar{\Gamma}_R - \Delta\bar{\Gamma}_L)$, defined as the difference between pump-probe response to right and left polarized light. In particular, with equivalent pump field amplitude \mathcal{E}_{pu} for both polarizations, we find

$$\Delta\bar{\Gamma}_{R-L}(2\Omega, \theta) \propto 2i \int d\omega_1 \mathbf{E}_{\text{pr}}(\omega_1) G_{\Omega\Omega}(\theta) \mathcal{E}_{\text{pu}}^2, \quad (\text{S30})$$

$$\Delta\bar{\Gamma}_{R-L}(-2\Omega, \theta) \propto -2i \int d\omega_1 \mathbf{E}_{\text{pr}}(\omega_1) G_{-\Omega-\Omega}(\theta) \mathcal{E}_{\text{pu}}^{*2}, \quad (\text{S31})$$

$$\Delta\bar{\Gamma}_{R-L}(0) \propto -2i \int d\omega_1 \mathbf{E}_{\text{pr}}(\omega_1) \chi_{ij}^A(\omega; \omega_1, \Omega, -\Omega) |\mathcal{E}_{\text{pu}}|^2. \quad (\text{S32})$$

We report in Table I the weights of the different spectral components, as obtained throughout this section, for $\theta = 0$ and monochromatic probe.

	Linearly polarized pump	Circularly polarized pump
$\omega_2 + \omega_3 = 2\Omega$	$\chi_{xy}^S [\sin(2\Delta\theta) (\mathcal{E}_S^2 - \mathcal{E}_P^2) + 2 \cos(2\Delta\theta) \mathcal{E}_P \mathcal{E}_S]$	$\chi_{xy}^S [\sin(2\Delta\theta) (\mathcal{E}_L^2 + \mathcal{E}_R^2) + i \cos(2\Delta\theta) (\mathcal{E}_L^2 - \mathcal{E}_R^2)]$
$\omega_2 + \omega_3 = -2\Omega$	$\chi_{xy}^S [\sin(2\Delta\theta) (\mathcal{E}_S^{*2} - \mathcal{E}_P^{*2}) + 2 \cos(2\Delta\theta) \mathcal{E}_P^* \mathcal{E}_S^*]$	$\chi_{xy}^S [\sin(2\Delta\theta) (\mathcal{E}_L^{*2} + \mathcal{E}_R^{*2}) - i \cos(2\Delta\theta) (\mathcal{E}_L^{*2} - \mathcal{E}_R^{*2})]$
$\omega_2 + \omega_3 = 0$	$\chi_{xy}^S [\sin(2\Delta\theta) (\mathcal{E}_S ^2 - \mathcal{E}_P ^2) + \cos(2\Delta\theta) (\mathcal{E}_P \mathcal{E}_S^* + \mathcal{E}_P^* \mathcal{E}_S)]$	$i\chi_{xy}^A (\mathcal{E}_L ^2 - \mathcal{E}_R ^2)$

Table I. Schematic recap of the field combinations that contribute to the pump-probe response components for $\theta = 0$.

RESPONSE TO MONOCHROMATIC PUMP PULSES WITH SMALL FREQUENCY MISMATCH

As reported in Ref. [23], when a frequency mismatch $\Delta\Omega$ between the two pump components $E_{\text{pu}}^P(\omega_s)$ and $E_{\text{pu}}^S(\omega_s)$ is present, a quasi-static response at $\Delta\Omega$ arises in the symmetric channel through difference-frequency generation of the circularly polarized pumps. Here we reproduce this result, and further show that the antisymmetric channel contributes exclusively to the quasi-static response for small mismatch $\Delta\Omega \ll \Omega$.

We again consider monochromatic fields, where now the P component is shifted by $-\Delta\Omega$,

$$\begin{aligned} E_{\text{pu}}^P(\omega_s) &= \mathcal{E}_P \delta(\omega_s - \Omega + \Delta\Omega) + \mathcal{E}_P^* \delta(\omega_s + \Omega - \Delta\Omega), \\ E_{\text{pu}}^S(\omega_s) &= \mathcal{E}_S \delta(\omega_s - \Omega) + \mathcal{E}_S^* \delta(\omega_s + \Omega), \end{aligned} \quad (\text{S33})$$

and then change basis with Eqs. (S23). As above, in the following we neglect terms that mix left and right pump components. With the frequency mismatch, Eqs. (S24), (S25) and (S26) are rewritten as

$$\begin{aligned} \mathcal{S}_{\parallel} &= -\frac{1}{2}(\mathcal{E}_L^2 + \mathcal{E}_R^2) [\delta(\omega_2 - \Omega)\delta(\omega_3 - \Omega) + \delta(\omega_2 - \Omega + \Delta\Omega)\delta(\omega_3 - \Omega + \Delta\Omega)] \\ &\quad -\frac{1}{2}(\mathcal{E}_L^{*2} + \mathcal{E}_R^{*2}) [\delta(\omega_2 + \Omega)\delta(\omega_3 + \Omega) + \delta(\omega_2 + \Omega - \Delta\Omega)\delta(\omega_3 + \Omega - \Delta\Omega)] \\ &\quad -\frac{1}{2}(|\mathcal{E}_L|^2 + |\mathcal{E}_R|^2) [\delta(\omega_2 - \Omega)\delta(\omega_3 + \Omega) + \delta(\omega_2 + \Omega)\delta(\omega_3 - \Omega) \\ &\quad \quad - \delta(\omega_2 - \Omega + \Delta\Omega)\delta(\omega_3 + \Omega - \Delta\Omega) - \delta(\omega_2 + \Omega - \Delta\Omega)\delta(\omega_3 - \Omega + \Delta\Omega)], \end{aligned} \quad (\text{S34})$$

$$\begin{aligned} \mathcal{S}_{\perp} &= -\frac{i}{2}(\mathcal{E}_L^2 - \mathcal{E}_R^2) [\delta(\omega_2 - \Omega + \Delta\Omega)\delta(\omega_3 - \Omega) + \delta(\omega_2 - \Omega)\delta(\omega_3 - \Omega + \Delta\Omega)] \\ &\quad +\frac{i}{2}(\mathcal{E}_L^{*2} - \mathcal{E}_R^{*2}) [\delta(\omega_2 + \Omega - \Delta\Omega)\delta(\omega_3 + \Omega) + \delta(\omega_2 + \Omega)\delta(\omega_3 + \Omega - \Delta\Omega)] \\ &\quad +\frac{i}{2}(|\mathcal{E}_L|^2 - |\mathcal{E}_R|^2) [\delta(\omega_2 - \Omega + \Delta\Omega)\delta(\omega_3 + \Omega) + \delta(\omega_2 + \Omega)\delta(\omega_3 - \Omega + \Delta\Omega) \\ &\quad \quad - \delta(\omega_2 - \Omega)\delta(\omega_3 + \Omega - \Delta\Omega) - \delta(\omega_2 + \Omega - \Delta\Omega)\delta(\omega_3 - \Omega)], \end{aligned} \quad (\text{S35})$$

and

$$\begin{aligned} \mathcal{A} &= -\frac{i}{2}(\mathcal{E}_L^2 - \mathcal{E}_R^2) [\delta(\omega_2 - \Omega + \Delta\Omega)\delta(\omega_3 - \Omega) - \delta(\omega_2 - \Omega)\delta(\omega_3 - \Omega + \Delta\Omega)] \\ &\quad +\frac{i}{2}(\mathcal{E}_L^{*2} - \mathcal{E}_R^{*2}) [\delta(\omega_2 + \Omega - \Delta\Omega)\delta(\omega_3 + \Omega) - \delta(\omega_2 + \Omega)\delta(\omega_3 + \Omega - \Delta\Omega)] \\ &\quad +\frac{i}{2}(|\mathcal{E}_L|^2 - |\mathcal{E}_R|^2) [\delta(\omega_2 - \Omega + \Delta\Omega)\delta(\omega_3 + \Omega) + \delta(\omega_2 - \Omega)\delta(\omega_3 + \Omega - \Delta\Omega) \\ &\quad \quad - \delta(\omega_2 + \Omega)\delta(\omega_3 - \Omega + \Delta\Omega) - \delta(\omega_2 + \Omega - \Delta\Omega)\delta(\omega_3 - \Omega)]. \end{aligned} \quad (\text{S36})$$

We now assume that the small frequency mismatch $\Delta\Omega \ll \Omega$ between the pump components does not significantly affect the third-order susceptibility, so that its dependence on $\Delta\Omega$ can be neglected, e.g., $\chi_{ij;kl}(\omega; \omega_1, \Omega, \Omega - \Delta\Omega) \simeq \chi_{ij;kl}(\omega; \omega_1, \Omega, \Omega)$ and analogously for all other combinations. Using Eqs. (S34), (S35) and (S36) in Eq. (S8) we find

$$\begin{aligned} \Delta\Gamma(t_{pp}, \theta) &\propto \int d\omega_1 E_{\text{pr}}(\omega_1) \\ &\quad \times \left[-F_{\Omega\Omega}(\theta) e^{-2i\Omega t_{pp}} (\mathcal{E}_L^2 + \mathcal{E}_R^2) (1 + e^{2i\Delta\Omega t_{pp}}) - F_{-\Omega-\Omega}(\theta) e^{2i\Omega t_{pp}} (\mathcal{E}_L^{*2} + \mathcal{E}_R^{*2}) (1 + e^{-2i\Delta\Omega t_{pp}}) \right. \\ &\quad \quad - 2iG_{\Omega\Omega}(\theta) (\mathcal{E}_L^2 - \mathcal{E}_R^2) e^{-i(2\Omega - \Delta\Omega)t_{pp}} + 2iG_{-\Omega-\Omega}(\theta) (\mathcal{E}_L^{*2} - \mathcal{E}_R^{*2}) e^{i(2\Omega - \Delta\Omega)t_{pp}} \\ &\quad \quad - 2(|\mathcal{E}_L|^2 - |\mathcal{E}_R|^2) (G_{\Omega-\Omega}(\theta) + G_{-\Omega\Omega}(\theta)) \sin(\Delta\Omega t_{pp}) \\ &\quad \quad \left. + 2i(|\mathcal{E}_L|^2 - |\mathcal{E}_R|^2) \chi_{ij}^A(\omega; \omega_1, \Omega, -\Omega) \cos(\Delta\Omega t_{pp}) \right]. \end{aligned} \quad (\text{S37})$$

As discussed above, contributions scaling with $\mathcal{E}_L^2 + \mathcal{E}_R^2$ and $\mathcal{E}_L^{*2} + \mathcal{E}_R^{*2}$ are canceled in the dichroic signal $\Delta\bar{\Gamma}_{R-L}$, so that only oscillations at $\pm(2\Omega - \Delta\Omega)$ and $\pm\Delta\Omega$ are present. In particular, in Fourier space,

$$\Delta\bar{\Gamma}_{R-L}(2\Omega - \Delta\Omega, \theta) \propto 2i \int d\omega_1 \text{E}_{\text{pr}}(\omega_1) G_{\Omega\Omega}(\theta) \mathcal{E}_{\text{pu}}^2 \quad (\text{S38})$$

$$\Delta\bar{\Gamma}_{R-L}(-2\Omega + \Delta\Omega, \theta) \propto -2i \int d\omega_1 \text{E}_{\text{pr}}(\omega_1) G_{-\Omega-\Omega}(\theta) \mathcal{E}_{\text{pu}}^{*2} \quad (\text{S39})$$

$$\Delta\bar{\Gamma}_{R-L}(\Delta\Omega, \theta) \propto -i \int d\omega_1 \text{E}_{\text{pr}}(\omega_1) [G_{\Omega-\Omega}(\theta) + G_{-\Omega\Omega}(\theta) + \chi_{ij}^A(\omega; \omega_1, \Omega, -\Omega)] |\mathcal{E}_{\text{pu}}|^2 \quad (\text{S40})$$

$$\Delta\bar{\Gamma}_{R-L}(-\Delta\Omega, \theta) \propto i \int d\omega_1 \text{E}_{\text{pr}}(\omega_1) [G_{\Omega-\Omega}(\theta) + G_{-\Omega\Omega}(\theta) - \chi_{ij}^A(\omega; \omega_1, \Omega, -\Omega)] |\mathcal{E}_{\text{pu}}|^2. \quad (\text{S41})$$

One can immediately see that a symmetric contribution to the quasi-static response, scaling with the coefficients $G_{kl}(\theta)$ in Eq. (S11), appears for finite $\Delta\Omega$. In particular, for $\theta = 0$, $G_{\Omega-\Omega}(0) + G_{-\Omega\Omega}(0) = \cos(2\Delta\theta) \chi_{ij}^S(\omega; \omega_1, \Omega, -\Omega)$, and one finds for the positive quasi-static component Eq. (S40)

$$\Delta\bar{\Gamma}_{R-L}(\Delta\Omega, \theta) \propto -i \int d\omega_1 \text{E}_{\text{pr}}(\omega_1) [\cos(2\Delta\theta) \chi_{ij}^S(\omega; \omega_1, \Omega, -\Omega) + \chi_{ij}^A(\omega; \omega_1, \Omega, -\Omega)] |\mathcal{E}_{\text{pu}}|^2. \quad (\text{S42})$$

On the other hand, the antisymmetric susceptibility does not contribute to the $\pm(2\Omega - \Delta\Omega)$ response. This remains valid as long as the susceptibility is approximately insensitive to the small frequency mismatch.

DETAILS OF THE CALCULATIONS ON THE sp -MODEL

Electronic Hamiltonian

For an explicit calculation of the antisymmetric susceptibility, we consider a simple square lattice with two atoms per unit cell, labeled A and B in the following. To simulate a system with distinct orbital character of the valence and the conduction band, we assign s -type orbitals to site A, with on-site energy $-\Delta$, and p_x and p_y orbitals to site B, with on-site energy $+\Delta$. Finally, we include nearest-neighbor hopping with amplitude t . The system is shown in Fig. 2(a) of the main text.

We define $a(\mathbf{R}_i)$ the annihilation operator on site A of the i -th unit cell, and $b_{x,y}(\mathbf{R}_i + \hat{x})$ the annihilation operator on site B of the same unit cell for orbitals p_x and p_y . Here we set the nearest-neighbor distance as 1. The Hamiltonian associated with this toy-model is, in real space,

$$\begin{aligned}
H = & -\Delta \sum_i [a^\dagger(\mathbf{R}_i)a(\mathbf{R}_i)] + \Delta \sum_i [b_x^\dagger(\mathbf{R}_i + \hat{x})b_x(\mathbf{R}_i + \hat{x}) + b_y^\dagger(\mathbf{R}_i + \hat{x})b_y(\mathbf{R}_i + \hat{x})] \\
& - t \sum_i [a^\dagger(\mathbf{R}_i)b_x(\mathbf{R}_i + \hat{x}) + b_x^\dagger(\mathbf{R}_i + \hat{x})a(\mathbf{R}_i)] - t \sum_i [a^\dagger(\mathbf{R}_i)b_y(\mathbf{R}_i + \hat{y}) + b_y^\dagger(\mathbf{R}_i + \hat{y})a(\mathbf{R}_i)] \\
& + t \sum_i [a^\dagger(\mathbf{R}_i)b_x(\mathbf{R}_i - \hat{x}) + b_x^\dagger(\mathbf{R}_i - \hat{x})a(\mathbf{R}_i)] + t \sum_i [a^\dagger(\mathbf{R}_i)b_y(\mathbf{R}_i - \hat{y}) + b_y^\dagger(\mathbf{R}_i - \hat{y})a(\mathbf{R}_i)]. \tag{S43}
\end{aligned}$$

Shifting to Fourier space, the Hamiltonian can be rewritten as

$$H = \sum_{\mathbf{k}} \begin{pmatrix} a_{\mathbf{k}}^\dagger & b_{x,\mathbf{k}}^\dagger & b_{y,\mathbf{k}}^\dagger \end{pmatrix} \mathcal{H}_{\mathbf{k}} \begin{pmatrix} a_{\mathbf{k}} \\ b_{x,\mathbf{k}} \\ b_{y,\mathbf{k}} \end{pmatrix}, \tag{S44}$$

where

$$\mathcal{H}_{\mathbf{k}} = \begin{pmatrix} -\Delta & -2it \sin(k_x) & -2it \sin(k_y) \\ 2it \sin(k_x) & +\Delta & 0 \\ 2it \sin(k_y) & 0 & +\Delta \end{pmatrix}. \tag{S45}$$

The tight-binding Hamiltonian describes three bands,

$$\begin{aligned}
E_{1,2}(\mathbf{k}) &= \mp \sqrt{\Delta^2 + 4t^2(\sin^2(k_x) + \sin^2(k_y))} \equiv \mp E_{\mathbf{k}}, \\
E_3(\mathbf{k}) &= \Delta. \tag{S46}
\end{aligned}$$

Band 1 displays dominant s -like character, whereas bands 2 and 3 display dominant p -like character.

We can then define the electronic Green's function as $\tilde{G}_0^{-1}(i\nu_n) = i\nu_n \mathbb{1} - \mathcal{H}_{\mathbf{k}}$, where $\mathbb{1}$ is the 2×2 identity matrix and $\nu_n = (2n + 1)\pi T$ is the fermionic Matsubara frequency at temperature T . Explicitly,

$$\tilde{G}_0(i\nu_n, \mathbf{k}) = \frac{1}{(i\nu_n - E_1(\mathbf{k}))(i\nu_n - E_2(\mathbf{k}))(i\nu_n - E_3(\mathbf{k}))} \begin{pmatrix} (i\nu_n - \Delta)^2 & (i\nu_n - \Delta)\epsilon_{k_x} & (i\nu_n - \Delta)\epsilon_{k_y} \\ (i\nu_n - \Delta)\epsilon_{k_x}^* & (i\nu_n)^2 - \Delta^2 - |\epsilon_{k_y}|^2 & \epsilon_{k_x}^* \epsilon_{k_y} \\ (i\nu_n - \Delta)\epsilon_{k_y}^* & \epsilon_{k_x} \epsilon_{k_y}^* & (i\nu_n)^2 - \Delta^2 - |\epsilon_{k_x}|^2 \end{pmatrix}, \tag{S47}$$

where we defined $\epsilon_{k_x} = -2it \sin(k_x)$ and $\epsilon_{k_y} = -2it \sin(k_y)$.

To represent the Green's function in the band basis in which it is diagonal, we perform the Bogoliubov rotation $\tilde{G}_0(i\nu_n, \mathbf{k}) = U_{\mathbf{k}} G_0(i\nu_n, \mathbf{k}) U_{\mathbf{k}}^\dagger$, and obtain

$$G_0(i\nu_n, \mathbf{k}) = \begin{pmatrix} \frac{1}{i\nu_n - E_1(\mathbf{k})} & 0 & 0 \\ 0 & \frac{1}{i\nu_n - E_2(\mathbf{k})} & 0 \\ 0 & 0 & \frac{1}{i\nu_n - E_3(\mathbf{k})} \end{pmatrix}. \tag{S48}$$

The matrix that performs the rotation reads explicitly

$$U_{\mathbf{k}} = \begin{pmatrix} u_{\mathbf{k}} & v_{\mathbf{k}} & 0 \\ \frac{\epsilon_{k_x}}{2E_{\mathbf{k}}u_{\mathbf{k}}} & \frac{\epsilon_{k_x}^*}{2E_{\mathbf{k}}v_{\mathbf{k}}} & \frac{\epsilon_{k_y}^*}{2E_{\mathbf{k}}u_{\mathbf{k}}v_{\mathbf{k}}} \\ \frac{\epsilon_{k_y}}{2E_{\mathbf{k}}u_{\mathbf{k}}} & \frac{\epsilon_{k_y}^*}{2E_{\mathbf{k}}v_{\mathbf{k}}} & \frac{\epsilon_{k_x}}{2E_{\mathbf{k}}u_{\mathbf{k}}v_{\mathbf{k}}} \end{pmatrix}, \quad (\text{S49})$$

where $u_{\mathbf{k}}$ and $v_{\mathbf{k}}$ are the coherence factors with properties $u_{\mathbf{k}}^2 + v_{\mathbf{k}}^2 = 1$, $u_{\mathbf{k}}^2 - v_{\mathbf{k}}^2 = \Delta/E_{\mathbf{k}}$, and $2u_{\mathbf{k}}v_{\mathbf{k}} = \sqrt{|\epsilon_{k_x}|^2 + |\epsilon_{k_y}|^2}/E_{\mathbf{k}}$.

Light-matter interaction

To introduce the electromagnetic field, represented by the vector potential \mathbf{A} , we perform the Peierls substitution $\mathbf{k} \rightarrow \mathbf{k} + \frac{e}{c}\mathbf{A}$ in the tight-binding Hamiltonian $\mathcal{H}_{\mathbf{k}}$ in Eq. (S45), with $-e$ the electron charge and c the light velocity. We then expand the resulting Hamiltonian in powers of \mathbf{A} , to generate all orders of light-matter interactions:

$$\mathcal{H}_{\mathbf{k} + \frac{e}{c}\mathbf{A}} \simeq \mathcal{H}_{\mathbf{k}} + \sum_n \frac{1}{n!} \frac{\partial^n \mathcal{H}_{\mathbf{k}}}{\partial \mathbf{k}^n} \cdot \left(\frac{e}{c} \mathbf{A} \right)^n. \quad (\text{S50})$$

Since we are interested in a third-order nonlinear response, relevant vertices are generated up to $n = 4$, which corresponds to taking 1-, 2-, 3- or 4-photons electronic transitions. For further simplification, we focus on the mixed components $\chi_{xy;xy}$ and $\chi_{xy;yx}$, relevant for the antisymmetric and symmetric susceptibilities, which means selecting processes involving two photons polarized along x and two along y . Since mixed derivatives of $\mathcal{H}_{\mathbf{k}}$ vanish in the sp -model by Eq. (S45), only one-photon (“paramagnetic”-like) terms and two-photons (“diamagnetic”-like) terms with photons of same polarization survive in the expansion. We note that to compute the $\chi_{xx;xx}$ component, relevant for the symmetric response at $\theta \neq 0$, 3- and 4-photon vertices need to be included to preserve gauge invariance of the final result. From Eq. (S45) we can find, in the orbital basis, the velocity vertices

$$\tilde{v}_x = \frac{\partial \mathcal{H}_{\mathbf{k}}}{\partial k_x} = \begin{pmatrix} 0 & -2it \cos(k_x) & 0 \\ 2it \cos(k_x) & 0 & 0 \\ 0 & 0 & 0 \end{pmatrix} \quad \tilde{v}_y = \frac{\partial \mathcal{H}_{\mathbf{k}}}{\partial k_y} = \begin{pmatrix} 0 & 0 & -2it \cos(k_y) \\ 0 & 0 & 0 \\ 2it \cos(k_y) & 0 & 0 \end{pmatrix} \quad (\text{S51})$$

that mediate paramagnetic interactions, and the density-like vertices

$$\tilde{\rho}_x = \frac{\partial^2 \mathcal{H}_{\mathbf{k}}}{\partial k_x^2} = \begin{pmatrix} 0 & 2it \sin(k_x) & 0 \\ -2it \sin(k_x) & 0 & 0 \\ 0 & 0 & 0 \end{pmatrix} \quad \tilde{\rho}_y = \frac{\partial^2 \mathcal{H}_{\mathbf{k}}}{\partial k_y^2} = \begin{pmatrix} 0 & 0 & 2it \sin(k_y) \\ 0 & 0 & 0 \\ -2it \sin(k_y) & 0 & 0 \end{pmatrix} \quad (\text{S52})$$

that mediate diamagnetic interactions. We can then represent these vertices in the band basis as $v_i = U_{\mathbf{k}}^\dagger \tilde{v}_i U_{\mathbf{k}}$ and $\rho_i = U_{\mathbf{k}}^\dagger \tilde{\rho}_i U_{\mathbf{k}}$ respectively. More generally, since eqs. (S51) and (S52) have the same matrix structure, one can recast the n -th order derivatives of the tight-binding Hamiltonian as

$$U_{\mathbf{k}}^\dagger \frac{\partial^n \mathcal{H}_{\mathbf{k}}}{\partial k_x^n} U_{\mathbf{k}} = \begin{pmatrix} \frac{\epsilon_{k_x}}{E_{\mathbf{k}}} & -\frac{\epsilon_{k_x}}{E_{\mathbf{k}}} \frac{\Delta}{\sqrt{|\epsilon_{k_x}|^2 + |\epsilon_{k_y}|^2}} & -\frac{\epsilon_{k_y}}{2E_{\mathbf{k}}v_{\mathbf{k}}} \\ -\frac{\epsilon_{k_x}}{E_{\mathbf{k}}} \frac{\Delta}{\sqrt{|\epsilon_{k_x}|^2 + |\epsilon_{k_y}|^2}} & -\frac{\epsilon_{k_x}}{E_{\mathbf{k}}} & -\frac{\epsilon_{k_y}}{2E_{\mathbf{k}}u_{\mathbf{k}}} \\ -\frac{\epsilon_{k_y}}{2E_{\mathbf{k}}v_{\mathbf{k}}} & -\frac{\epsilon_{k_y}}{2E_{\mathbf{k}}u_{\mathbf{k}}} & 0 \end{pmatrix} \frac{\partial^n \epsilon_{k_x}}{\partial k_x^n}, \quad (\text{S53})$$

and

$$U_{\mathbf{k}}^\dagger \frac{\partial^n \mathcal{H}_{\mathbf{k}}}{\partial k_y^n} U_{\mathbf{k}} = \begin{pmatrix} \frac{\epsilon_{k_y}}{E_{\mathbf{k}}} & -\frac{\epsilon_{k_y}}{E_{\mathbf{k}}} \frac{\Delta}{\sqrt{|\epsilon_{k_x}|^2 + |\epsilon_{k_y}|^2}} & -\frac{\epsilon_{k_x}}{2E_{\mathbf{k}}v_{\mathbf{k}}} \\ -\frac{\epsilon_{k_y}}{E_{\mathbf{k}}} \frac{\Delta}{\sqrt{|\epsilon_{k_x}|^2 + |\epsilon_{k_y}|^2}} & -\frac{\epsilon_{k_y}}{E_{\mathbf{k}}} & -\frac{\epsilon_{k_x}}{2E_{\mathbf{k}}u_{\mathbf{k}}} \\ -\frac{\epsilon_{k_x}}{2E_{\mathbf{k}}v_{\mathbf{k}}} & -\frac{\epsilon_{k_x}}{2E_{\mathbf{k}}u_{\mathbf{k}}} & 0 \end{pmatrix} \frac{\partial^n \epsilon_{k_y}}{\partial k_y^n}. \quad (\text{S54})$$

Having selected the relevant terms from the interaction Hamiltonian Eq. (S50), we can employ a path-integral formalism in which the system is described by the partition function $\mathcal{Z} = \int \mathcal{D}[\psi] \mathcal{D}[\mathbf{A}] e^{-S[\psi, \mathbf{A}]}$, where ψ is the

electron spinor field defined by Eq. (S44). The total light-matter action reads

$$S[\psi, \mathbf{A}] = - \sum_{i\nu_n, \mathbf{k}} \psi_{\mathbf{k}}^T(-i\nu_n) \tilde{G}_0^{-1}(i\nu_n, \mathbf{k}) \psi_{\mathbf{k}}(i\nu_n) + \sum_{i\nu_n, \mathbf{k}} \sum_{i\nu'_n, \mathbf{k}'} \psi_{\mathbf{k}}^T(-i\nu_n) \Sigma_{\mathbf{k}\mathbf{k}'}(i\nu_n - i\nu'_n) \psi_{\mathbf{k}'}(i\nu'_n), \quad (\text{S55})$$

with

$$\Sigma_{\mathbf{k}\mathbf{k}'}(i\nu_n - i\nu'_n) = \delta_{\mathbf{k}\mathbf{k}'} \left[\sqrt{\frac{T}{N}} \frac{e}{c} \sum_{i\Omega_m} [\tilde{v}_x A_x(i\Omega_m) + \tilde{v}_y A_y(i\Omega_m)] \delta(i\Omega_m - i\nu_n + i\nu'_n) \right. \\ \left. + \frac{T}{N} \frac{e^2}{2c^2} \sum_{i\Omega_m} \sum_{i\Omega_n} [\tilde{\rho}_x A_x(i\Omega_m) A_x(i\Omega_n) + \tilde{\rho}_y A_y(i\Omega_m) A_y(i\Omega_n)] \delta(i\Omega_m + i\Omega_n - i\nu_n + i\nu'_n) \right], \quad (\text{S56})$$

where $\Omega_m = 2\pi mT$ are the bosonic Matsubara frequencies, and N the number of unit cells. Following the standard procedure established in Refs. [27, 28], we then integrate the electron field out of the partition function, to find the matter-mediated contribution to the effective action of the electromagnetic field:

$$S_{\text{eff}}[\mathbf{A}] = \sum_{m \geq 1} \frac{\text{Tr}[\tilde{G}_0 \Sigma]^m}{m}, \quad (\text{S57})$$

where Tr is the trace, and retain only terms scaling with $A_x^2 A_y^2$, that describe mixed third-order processes mediated by electronic transitions.

Diamagnetic-like antisymmetric kernel

The diamagnetic-like contribution is contained in the $m = 2$ term of $S_{\text{eff}}[\mathbf{A}]$ in Eq. (S57), when multiplying twice the second row of Eq. (S56). In particular, we are interested in

$$S_{\text{dia}}[\mathbf{A}] = \frac{e^4}{4c^4} \sum_{i\Omega_m} \sum_{i\Omega_n} \sum_{i\Omega_l} \sum_{i\Omega_s} \frac{T}{N} \sum_{i\nu_n, \mathbf{k}} \text{Tr}[\tilde{G}_0(i\nu_n, \mathbf{k}) \tilde{\rho}_y \tilde{G}_0(i\nu_n + i\Omega_m + i\Omega_n, \mathbf{k}) \tilde{\rho}_x] \\ \times A_y(i\Omega_m) A_y(i\Omega_n) A_x(i\Omega_l) A_x(i\Omega_s) \delta_{-i\Omega_s, i\Omega_m + i\Omega_n + i\Omega_l}, \quad (\text{S58})$$

where $i\Omega_m + i\Omega_n + i\Omega_l + i\Omega_s = 0$ by energy conservation. We then rotate both the Green's function and the density-like vertex to the band basis, and explicit the trace:

$$\text{Tr}[\tilde{G}_0(i\nu_n, \mathbf{k}) \tilde{\rho}_y \tilde{G}_0(i\nu_n + i\Omega_m + i\Omega_n, \mathbf{k}) \tilde{\rho}_x] \\ = \text{Tr}[G_0(i\nu_n, \mathbf{k}) \rho_y G_0(i\nu_n + i\Omega_m + i\Omega_n, \mathbf{k}) \rho_x] \\ = \sum_{ab} [G_0(i\nu_n, \mathbf{k})]_{aa} [\rho_y]_{ab} [G_0(i\nu_n + i\Omega_m + i\Omega_n, \mathbf{k})]_{bb} [\rho_x]_{ba}, \quad (\text{S59})$$

where a and b run over band indices. We can thus rewrite the diamagnetic action as

$$S_{\text{dia}}[\mathbf{A}] = \frac{e^4}{4c^4} \sum_{i\Omega_m} \sum_{i\Omega_n} \sum_{i\Omega_l} \sum_{i\Omega_s} \sum_{ab} \left[[\rho_y]_{ab} [\rho_x]_{ba} d_{ab}(i\Omega_m + i\Omega_n) \right] A_y(i\Omega_m) A_y(i\Omega_n) A_x(i\Omega_l) A_x(i\Omega_s) \delta_{-i\Omega_s, i\Omega_m + i\Omega_n + i\Omega_l}, \quad (\text{S60})$$

where

$$d_{ab}(i\Omega_m + i\Omega_n) = \frac{T}{N} \sum_{i\nu_n, \mathbf{k}} [G_0(i\nu_n, \mathbf{k})]_{aa} [G_0(i\nu_n + i\Omega_m + i\Omega_n, \mathbf{k})]_{bb} \\ = \frac{1}{N} \sum_{\mathbf{k}} \frac{f(E_a(\mathbf{k})) - f(E_b(\mathbf{k}))}{i\Omega_m + i\Omega_n - (E_b(\mathbf{k}) - E_a(\mathbf{k}))} \quad (\text{S61})$$

contains the frequency-dependent poles associated with the electronic transitions, with $f(E_a(\mathbf{k}))$ the Fermi-Dirac distribution. We now compute the third-order nonlinear current, that describes the response of the system, as the

functional derivative of Eq. (S60) with respect to A_x/c :

$$J_x(\omega) \propto -\frac{\delta S_{\text{dia}}[\mathbf{A}]}{\delta A_x(-\omega)/c} = -\frac{e^4}{2c^3} \int d\omega_1 d\omega_2 d\omega_3 \sum_{ab} \left[[\rho_y]_{ab} [\rho_x]_{ba} d_{ab}(\omega_1 + \omega_2) \right] A_y(\omega_1) A_y(\omega_2) A_x(\omega_3) \delta(\omega_1 + \omega_2 + \omega_3 - \omega), \quad (\text{S62})$$

where we performed the analytic continuation for all bosonic Matsubara frequencies, and $\omega_1 + \omega_2 + \omega_3 - \omega = 0$ by energy conservation. So far, we did not distinguish explicitly between pump and probe fields when writing the vector potentials A_i . According to the convention established in the main text, we are interested in a nonlinear current along x , generated in response to a probe along y and a circular pump having both x and y components. Thus, the functional derivative in Eq. (S62) is performed with respect to the generated signal along x , and the remaining three fields are associated with a probe photon A_x and two pump photons A_x and A_y . The kernel component $K_{xy;yx}^{\text{dia}}(\omega; \omega_1, \omega_2, \omega_3)$ is obtained as the coefficient of $(A/c)^3$ in the nonlinear current.

We now consider monochromatic pump and probe fields. For the antisymmetric kernel, we are interested in computing $K_{xy;xy}(\omega; \omega, \Omega, -\Omega) = K_{xy;yx}(\omega; \omega, -\Omega, \Omega)$, and $K_{xy;yx}(\omega; \omega, \Omega, -\Omega)$. When $\omega_2 = \Omega$ and $\omega_3 = -\Omega$, we obtain from the nonlinear current

$$K_{xy;yx}^{\text{dia}}(\omega; \omega, \Omega, -\Omega) = -\frac{e^4}{2} \sum_{ab} [\rho_y]_{ab} [\rho_x]_{ba} d_{ab}(\omega + \Omega), \quad (\text{S63})$$

while, for $\omega_2 = -\Omega$ and $\omega_3 = \Omega$,

$$K_{xy;yx}^{\text{dia}}(\omega; \omega, -\Omega, \Omega) = K_{xy;xy}^{\text{dia}}(\omega; \omega, \Omega, -\Omega) = -\frac{e^4}{2} \sum_{ab} [\rho_y]_{ab} [\rho_x]_{ba} d_{ab}(\omega - \Omega). \quad (\text{S64})$$

Finally, using the symmetry properties of the kernel, we can write the antisymmetric diamagnetic component as

$$\begin{aligned} K_{\text{dia}}^A(\omega; \omega, \Omega, -\Omega) &= K_{xy;xy}^{\text{dia}}(\omega; \omega, \Omega, -\Omega) - K_{xy;yx}^{\text{dia}}(\omega; \omega, \Omega, -\Omega) \\ &= \frac{1}{2} [K_{xy;xy}^{\text{dia}}(\omega; \omega, \Omega, -\Omega) - K_{xy;yx}^{\text{dia}}(\omega; \omega, \Omega, -\Omega) + K_{yx;yx}^{\text{dia}}(\omega; \omega, \Omega, -\Omega) - K_{yx;xy}^{\text{dia}}(\omega; \omega, \Omega, -\Omega)] \\ &= -\frac{e^4}{4} \sum_{ab} [[\rho_x]_{ab} [\rho_y]_{ba} + [\rho_y]_{ab} [\rho_x]_{ba}] [d_{ab}(\omega - \Omega) - d_{ab}(\omega + \Omega)], \end{aligned} \quad (\text{S65})$$

which corresponds to Eq. (9) of the main text.

For simulations of the antisymmetric susceptibility we set $T = 0$, so that the Fermi-Dirac distributions in (S61) for the three bands are $f(E_1(\mathbf{k})) = 1$, $f(E_{2,3}(\mathbf{k})) = 0$. The sum over \mathbf{k} is, instead, performed numerically.

Paramagnetic-like antisymmetric kernel

The paramagnetic-like contribution is contained in the $m = 4$ term of $S_{\text{eff}}[\mathbf{A}]$ in Eq. (S57), when multiplying four times the first row of Eq. (S56). In particular, we are interested in

$$\begin{aligned} S_{\text{para}}[\mathbf{A}] &= \frac{e^4}{4c^4} \sum_{i\Omega_m} \sum_{i\Omega_n} \sum_{i\Omega_l} \sum_{i\Omega_s} \\ &\quad \frac{T}{N} \sum_{i\nu_n, \mathbf{k}} \text{Tr} [\tilde{G}_0(i\nu_n, \mathbf{k}) \tilde{v}_y \tilde{G}_0(i\nu_n + i\Omega_m, \mathbf{k}) \tilde{v}_y \tilde{G}_0(i\nu_n + i\Omega_m + i\Omega_n, \mathbf{k}) \tilde{v}_x \tilde{G}_0(i\nu_n + i\Omega_m + i\Omega_n + i\Omega_l, \mathbf{k}) \tilde{v}_x] \\ &\quad \times A_y(i\Omega_m) A_y(i\Omega_n) A_x(i\Omega_l) A_x(i\Omega_s) \delta_{-i\Omega_s, i\Omega_m + i\Omega_n + i\Omega_l} + \text{perm.}, \end{aligned} \quad (\text{S66})$$

where ‘‘perm.’’ denotes all distinct permutations of the external field insertions, i.e., all possible ways of attaching the photon legs to the fermionic loop. We note that every permutation also changes the position of the velocity vertices in the trace, accordingly. Following the same steps of the diamagnetic-like case, we rewrite the trace as

$$\begin{aligned} &\text{Tr} [\tilde{G}_0(i\nu_n, \mathbf{k}) \tilde{v}_y \tilde{G}_0(i\nu_n + i\Omega_m, \mathbf{k}) \tilde{v}_y \tilde{G}_0(i\nu_n + i\Omega_m + i\Omega_n, \mathbf{k}) \tilde{v}_x \tilde{G}_0(i\nu_n + i\Omega_m + i\Omega_n + i\Omega_l, \mathbf{k}) \tilde{v}_x] \\ &= \text{Tr} [G_0(i\nu_n, \mathbf{k}) \mathbf{v}_y G_0(i\nu_n + i\Omega_m, \mathbf{k}) \mathbf{v}_y G_0(i\nu_n + i\Omega_m + i\Omega_n, \mathbf{k}) \mathbf{v}_x G_0(i\nu_n + i\Omega_m + i\Omega_n + i\Omega_l, \mathbf{k}) \mathbf{v}_x] \\ &= \sum_{abcd} [G_0(i\nu_n, \mathbf{k})]_{aa} [\mathbf{v}_y]_{ab} [G_0(i\nu_n + i\Omega_m, \mathbf{k})]_{bb} [\mathbf{v}_y]_{bc} \\ &\quad \times [G_0(i\nu_n + i\Omega_m + i\Omega_n, \mathbf{k})]_{cc} [\mathbf{v}_x]_{cd} [G_0(i\nu_n + i\Omega_m + i\Omega_n + i\Omega_l, \mathbf{k})]_{dd} [\mathbf{v}_x]_{da}, \end{aligned} \quad (\text{S67})$$

where $a, b, c,$ and d run over band indices. The paramagnetic contribution to the action can then be rewritten as

$$S_{\text{para}}[\mathbf{A}] = \frac{e^4}{4c^2} \sum_{i\Omega_m} \sum_{i\Omega_n} \sum_{i\Omega_l} \sum_{i\Omega_s} \sum_{abcd} \left[[v_y]_{ab} [v_y]_{bc} [v_x]_{cd} [v_x]_{da} p_{abcd}(i\Omega_m, i\Omega_n, i\Omega_l) \right] \\ \times A_y(i\Omega_m) A_y(i\Omega_n) A_x(i\Omega_l) A_x(i\Omega_s) \delta_{-i\Omega_s, i\Omega_m + i\Omega_n + i\Omega_l} + \text{perm.}, \quad (\text{S68})$$

where

$$p_{abcd}(i\Omega_m, i\Omega_n, i\Omega_l) = \frac{T}{N} \sum_{i\nu_n, \mathbf{k}} [G_0(i\nu_n, \mathbf{k})]_{aa} [G_0(i\nu_n + i\Omega_m, \mathbf{k})]_{bb} \\ \times [G_0(i\nu_n + i\Omega_m + i\Omega_n, \mathbf{k})]_{cc} [G_0(i\nu_n + i\Omega_m + i\Omega_n + i\Omega_l, \mathbf{k})]_{dd} \\ = -\frac{1}{N} \sum_{\mathbf{k}} \left[\frac{f(E_a(\mathbf{k}))}{(i\Omega_m + E_a(\mathbf{k}) - E_b(\mathbf{k}))(i\Omega_m + i\Omega_n + E_a(\mathbf{k}) - E_c(\mathbf{k}))(i\Omega_m + i\Omega_n + i\Omega_l + E_a(\mathbf{k}) - E_d(\mathbf{k}))} \right. \\ + \frac{f(E_b(\mathbf{k}))}{(-i\Omega_m + E_b(\mathbf{k}) - E_a(\mathbf{k}))(i\Omega_n + E_b(\mathbf{k}) - E_c(\mathbf{k}))(i\Omega_n + i\Omega_l + E_b(\mathbf{k}) - E_d(\mathbf{k}))} \\ + \frac{f(E_c(\mathbf{k}))}{(-i\Omega_m - i\Omega_n + E_c(\mathbf{k}) - E_a(\mathbf{k}))(-i\Omega_n + E_c(\mathbf{k}) - E_b(\mathbf{k}))(i\Omega_l + E_c(\mathbf{k}) - E_d(\mathbf{k}))} \\ \left. + \frac{f(E_d(\mathbf{k}))}{(-i\Omega_m - i\Omega_n - i\Omega_l + E_d(\mathbf{k}) - E_a(\mathbf{k}))(-i\Omega_n - i\Omega_l + E_d(\mathbf{k}) - E_b(\mathbf{k}))(-i\Omega_l + E_d(\mathbf{k}) - E_c(\mathbf{k}))} \right] \quad (\text{S69})$$

contains the frequency-dependent poles, analogously to d_{ab} for the diamagnetic process. From Eq. (S68) we can compute the nonlinear current:

$$\mathbf{J}_x(\omega) \propto -\frac{\delta S_{\text{para}}[\mathbf{A}]}{\delta A_x(-\omega)/c} = -\frac{e^4}{2c^3} \int d\omega_1 d\omega_2 d\omega_3 \sum_{abcd} \left[[v_y]_{ab} [v_y]_{bc} [v_x]_{cd} [v_x]_{da} p_{abcd}(\omega_1, \omega_2, \omega_3) \right] \\ \times A_y(\omega_1) A_y(\omega_2) A_x(\omega_3) \delta(\omega_1 + \omega_2 + \omega_3 - \omega) + \text{perm.}, \quad (\text{S70})$$

where we performed the analytic continuation for all bosonic Matsubara frequencies and $\omega_1 + \omega_2 + \omega_3 - \omega = 0$. The kernel component $\mathbf{K}_{xy;yx}^{\text{para}}(\omega; \omega_1, \omega_2, \omega_3)$ is obtained as the coefficient of $(A/c)^3$ in the nonlinear current.

We now consider monochromatic fields. With the ultimate goal of obtaining compact expressions for the antisymmetric kernel, it is convenient to write all six permutations in the kernel components explicitly. In particular,

$$\mathbf{K}_{xy;yx}^{\text{para}}(\omega; \omega, \Omega, -\Omega) = -\frac{e^4}{2} \sum_{abcd} \left[[v_y]_{ab} [v_y]_{bc} [v_x]_{cd} [v_x]_{da} p_{abcd}(\omega, \Omega, -\Omega) \right. \\ + [v_y]_{ab} [v_y]_{bc} [v_x]_{cd} [v_x]_{da} p_{abcd}(\Omega, \omega, -\Omega) \\ + [v_x]_{ab} [v_y]_{bc} [v_y]_{cd} [v_x]_{da} p_{abcd}(-\Omega, \Omega, \omega) \\ + [v_x]_{ab} [v_y]_{bc} [v_y]_{cd} [v_x]_{da} p_{abcd}(-\Omega, \omega, \Omega) \\ + [v_y]_{ab} [v_x]_{bc} [v_y]_{cd} [v_x]_{da} p_{abcd}(\Omega, -\Omega, \omega) \\ \left. + [v_y]_{ab} [v_x]_{bc} [v_y]_{cd} [v_x]_{da} p_{abcd}(\omega, -\Omega, \Omega) \right] \quad (\text{S71})$$

for $\omega_2 = \Omega$ and $\omega_3 = -\Omega$, and

$$\mathbf{K}_{xy;yx}^{\text{para}}(\omega; \omega, -\Omega, \Omega) = \mathbf{K}_{xy;xy}^{\text{para}}(\omega; \omega, \Omega, -\Omega) = -\frac{e^4}{2} \sum_{abcd} \left[[v_y]_{ab} [v_x]_{bc} [v_y]_{cd} [v_x]_{da} p_{abcd}(\omega, \Omega, -\Omega) \right. \\ + [v_x]_{ab} [v_y]_{bc} [v_y]_{cd} [v_x]_{da} p_{abcd}(\Omega, \omega, -\Omega) \\ + [v_y]_{ab} [v_x]_{bc} [v_y]_{cd} [v_x]_{da} p_{abcd}(-\Omega, \Omega, \omega) \\ + [v_y]_{ab} [v_y]_{bc} [v_x]_{cd} [v_x]_{da} p_{abcd}(-\Omega, \omega, \Omega) \\ + [v_x]_{ab} [v_y]_{bc} [v_y]_{cd} [v_x]_{da} p_{abcd}(\Omega, -\Omega, \omega) \\ \left. + [v_y]_{ab} [v_y]_{bc} [v_x]_{cd} [v_x]_{da} p_{abcd}(\omega, -\Omega, \Omega) \right] \quad (\text{S72})$$

for $\omega_2 = -\Omega$ and $\omega_3 = \Omega$. Notice that in every term the last matrix element $[\mathbf{v}_x]_{da}$ is fixed on the x component by our choice of performing the detection along x . Finally, we define the vectors $\mathbf{v} = (v_x, v_y)$ and make use of the symmetry properties of the kernel to write the antisymmetric paramagnetic component as

$$\begin{aligned}
K_{\text{para}}^{\mathbf{A}}(\omega; \omega, \Omega, -\Omega) &= K_{xy;xy}^{\text{para}}(\omega; \omega, \Omega, -\Omega) - K_{xy;yx}^{\text{para}}(\omega; \omega, \Omega, -\Omega) \\
&= \frac{1}{2} [K_{xy;xy}^{\text{para}}(\omega; \omega, \Omega, -\Omega) - K_{xy;yx}^{\text{para}}(\omega; \omega, \Omega, -\Omega) + K_{yx;yx}^{\text{para}}(\omega; \omega, \Omega, -\Omega) - K_{yx;xy}^{\text{para}}(\omega; \omega, \Omega, -\Omega)] \\
&= -\frac{e^4}{4} \sum_{abcd} [([\mathbf{v}]_{ab} \times [\mathbf{v}]_{bc}) \cdot ([\mathbf{v}]_{cd} \times [\mathbf{v}]_{da})] [p_{abcd}(-\Omega, \Omega, \omega) - p_{abcd}(\Omega, -\Omega, \omega)] \\
&\quad + [([\mathbf{v}]_{ab} \times [\mathbf{v}]_{cd}) \cdot ([\mathbf{v}]_{bc} \times [\mathbf{v}]_{da})] [p_{abcd}(-\Omega, \omega, \Omega) - p_{abcd}(\Omega, \omega, -\Omega)] \\
&\quad + [([\mathbf{v}]_{bc} \times [\mathbf{v}]_{cd}) \cdot ([\mathbf{v}]_{ab} \times [\mathbf{v}]_{da})] [p_{abcd}(\omega, -\Omega, \Omega) - p_{abcd}(\omega, \Omega, -\Omega)], \tag{S73}
\end{aligned}$$

which corresponds to Eq. (10) of the main text.

As it is the case for the diamagnetic kernel, the explicit calculation of Eq. (S69) is carried out at $T = 0$, and the sum over \mathbf{k} is performed numerically.

Mixed diamagnetic-paramagnetic antisymmetric kernel

The mixed contributions with one diamagnetic and two paramagnetic insertions are contained in the $m = 3$ term of $S_{\text{eff}}[\mathbf{A}]$ in Eq. (S57), when multiplying the first twice the first row and once the second row of Eq. (S56). In particular, we are interested in

$$\begin{aligned}
S_{\text{mix}}^{(1)}[\mathbf{A}] &= \frac{e^4}{6c^4} \sum_{i\Omega_m} \sum_{i\Omega_n} \sum_{i\Omega_l} \sum_{i\Omega_s} \frac{T}{N} \sum_{i\nu_n, \mathbf{k}} \text{Tr} [\tilde{G}_0(i\nu_n, \mathbf{k}) \tilde{v}_y \tilde{G}_0(i\nu_n + i\Omega_m, \mathbf{k}) \tilde{v}_y \tilde{G}_0(i\nu_n + i\Omega_m + i\Omega_n, \mathbf{k}) \tilde{\rho}_x] \\
&\quad \times A_y(i\Omega_m) A_y(i\Omega_n) A_x(i\Omega_l) A_x(i\Omega_s) \delta_{-i\Omega_s, i\Omega_m + i\Omega_n + i\Omega_l} \tag{S74}
\end{aligned}$$

and

$$\begin{aligned}
S_{\text{mix}}^{(2)}[\mathbf{A}] &= \frac{e^4}{6c^4} \sum_{i\Omega_m} \sum_{i\Omega_n} \sum_{i\Omega_l} \sum_{i\Omega_s} \frac{T}{N} \sum_{i\nu_n, \mathbf{k}} \text{Tr} [\tilde{G}_0(i\nu_n, \mathbf{k}) \tilde{\rho}_y \tilde{G}_0(i\nu_n + i\Omega_m + i\Omega_n, \mathbf{k}) \tilde{v}_x \tilde{G}_0(i\nu_n + i\Omega_m + i\Omega_n + i\Omega_l, \mathbf{k}) \tilde{v}_x] \\
&\quad \times A_y(i\Omega_m) A_y(i\Omega_n) A_x(i\Omega_l) A_x(i\Omega_s) \delta_{-i\Omega_s, i\Omega_m + i\Omega_n + i\Omega_l}. \tag{S75}
\end{aligned}$$

The two actions have been explicitly separated having in mind that the detection along x can be performed either on the diamagnetic insertion (process $S_{\text{mix}}^{(1)}$) or on a paramagnetic one (process $S_{\text{mix}}^{(2)}$). In the following we provide details for the calculation of the first contribution.

Following the same strategy detailed above, we rewrite the trace as

$$\begin{aligned}
&\text{Tr} [\tilde{G}_0(i\nu_n, \mathbf{k}) \tilde{v}_y \tilde{G}_0(i\nu_n + i\Omega_m, \mathbf{k}) \tilde{v}_y \tilde{G}_0(i\nu_n + i\Omega_m + i\Omega_n, \mathbf{k}) \tilde{\rho}_x] \\
&= \text{Tr} [G_0(i\nu_n, \mathbf{k}) v_y G_0(i\nu_n + i\Omega_m, \mathbf{k}) v_y G_0(i\nu_n + i\Omega_m + i\Omega_n, \mathbf{k}) \rho_x] \\
&= \sum_{abc} [G_0(i\nu_n, \mathbf{k})]_{aa} [v_y]_{ab} [G_0(i\nu_n + i\Omega_m, \mathbf{k})]_{bb} [v_y]_{bc} [G_0(i\nu_n + i\Omega_m + i\Omega_n, \mathbf{k})]_{cc} [\rho_x]_{ca}, \tag{S76}
\end{aligned}$$

where a , b , and c run over band indices. The mixed action can thus be rewritten as

$$S_{\text{mix}}^{(1)}[\mathbf{A}] = \frac{e^4}{6c^4} \sum_{i\Omega_m} \sum_{i\Omega_n} \sum_{i\Omega_l} \sum_{abc} [v_y]_{ab} [v_y]_{bc} [\rho_x]_{ca} m_{abc}(i\Omega_m, i\Omega_m + i\Omega_n) A_y(i\Omega_m) A_y(i\Omega_n) A_x(i\Omega_l) A_x(i\Omega_s), \tag{S77}$$

where

$$\begin{aligned}
m_{abc}(i\Omega_m, i\Omega_m + i\Omega_n) &= \frac{T}{N} \sum_{i\nu_n, \mathbf{k}} [G_0(i\nu_n, \mathbf{k})]_{aa} [G_0(i\nu_n + i\Omega_m, \mathbf{k})]_{bb} [G_0(i\nu_n + i\Omega_m + i\Omega_n, \mathbf{k})]_{cc} \\
&= -\frac{1}{N} \sum_{\mathbf{k}} \left[\frac{f(E_a(\mathbf{k}))}{(i\Omega_m + E_a(\mathbf{k}) - E_b(\mathbf{k}))(i\Omega_m + i\Omega_n + E_a(\mathbf{k}) - E_c(\mathbf{k}))} \right. \\
&\quad + \frac{f(E_b(\mathbf{k}))}{(-i\Omega_m + E_b(\mathbf{k}) - E_a(\mathbf{k}))(-i\Omega_m + (i\Omega_m + i\Omega_n) + E_b(\mathbf{k}) - E_c(\mathbf{k}))} \\
&\quad \left. + \frac{f(E_c(\mathbf{k}))}{(-i\Omega_m - i\Omega_n + E_c(\mathbf{k}) - E_a(\mathbf{k}))(i\Omega_m - (i\Omega_m + i\Omega_n) + E_c(\mathbf{k}) - E_b(\mathbf{k}))} \right] \quad (\text{S78})
\end{aligned}$$

contains the frequency dependent poles, analogously to d_{ab} and p_{abcd} . From Eq. (S77) we can compute the nonlinear current:

$$\begin{aligned}
\mathbf{J}_x^{(1)}(\omega) &\propto -\frac{\delta S_{\text{mix}}^{(1)}[\mathbf{A}]}{\delta \mathbf{A}_x(-\omega)/c} \\
&= -\frac{e^4}{3c^3} \int d\omega_1 d\omega_2 d\omega_3 \sum_{abc} \left[[v_y]_{ab} [v_y]_{bc} [\rho_x]_{ca} m_{abc}(\omega_1, \omega_1 + \omega_2) \right] A_y(\omega_1) A_y(\omega_2) A_x(\omega_3) \delta(\omega_1 + \omega_2 + \omega_3 - \omega), \quad (\text{S79})
\end{aligned}$$

where we performed the analytic continuation for all bosonic Matsubara frequencies and $\omega_1 + \omega_2 + \omega_3 - \omega = 0$. The coefficient of $(A/c)^3$ yields the kernel component $\mathbf{K}_{xy;yx}^{\text{mix}(1)}(\omega; \omega_1, \omega_2, \omega_3)$. With monochromatic fields, we obtain

$$\mathbf{K}_{xy;yx}^{\text{mix}(1)}(\omega; \omega, \Omega, -\Omega) = -\frac{e^4}{3} \sum_{abc} [v_y]_{ab} [v_y]_{bc} [\rho_x]_{ca} m_{abc}(\omega, \omega + \Omega), \quad (\text{S80})$$

for $\omega_2 = \Omega$ and $\omega_3 = -\Omega$, and

$$\mathbf{K}_{xy;yx}^{\text{mix}(1)}(\omega; \omega, -\Omega, \Omega) = \mathbf{K}_{xy;xy}^{\text{mix}(1)}(\omega; \omega, \Omega, -\Omega) = -\frac{e^4}{3} \sum_{abc} [v_y]_{ab} [v_y]_{bc} [\rho_x]_{ca} m_{abc}(\omega, \omega - \Omega), \quad (\text{S81})$$

for $\omega_2 = -\Omega$ and $\omega_3 = \Omega$. We can finally write the first antisymmetric mixed component as

$$\begin{aligned}
\mathbf{K}_{\text{mix}}^{\mathcal{A}(1)}(\omega; \omega, \Omega, -\Omega) &= \mathbf{K}_{xy;xy}^{\text{mix}(1)}(\omega; \omega, \Omega, -\Omega) - \mathbf{K}_{xy;yx}^{\text{mix}(1)}(\omega; \omega, \Omega, -\Omega) \\
&= \frac{1}{2} [\mathbf{K}_{xy;xy}^{\text{mix}(1)}(\omega; \omega, \Omega, -\Omega) - \mathbf{K}_{xy;yx}^{\text{mix}(1)}(\omega; \omega, \Omega, -\Omega) + \mathbf{K}_{yx;yx}^{\text{mix}(1)}(\omega; \omega, \Omega, -\Omega) - \mathbf{K}_{yx;xy}^{\text{mix}(1)}(\omega; \omega, \Omega, -\Omega)] \\
&= -\frac{e^4}{6} \sum_{abc} [[v_x]_{ab} [v_x]_{bc} [\rho_y]_{ca} + [v_y]_{ab} [v_y]_{bc} [\rho_x]_{ca}] [m_{abc}(\omega, \omega - \Omega) - m_{abc}(\omega, \omega + \Omega)]. \quad (\text{S82})
\end{aligned}$$

Completely analogous calculations on the second contribution, from Eq. (S75), give

$$\mathbf{K}_{\text{mix}}^{\mathcal{A}(2)}(\omega; \omega, \Omega, -\Omega) = -\frac{e^4}{6} \sum_{abc} [[\rho_x]_{ab} [v_y]_{bc} [v_y]_{ca} + [\rho_y]_{ab} [v_x]_{bc} [v_x]_{ca}] [m_{abc}(\omega - \Omega, \omega) - m_{abc}(\omega + \Omega, \omega)]. \quad (\text{S83})$$

The total mixed diamagnetic-paramagnetic antisymmetric kernel is then found as

$$\mathbf{K}_{\text{mix}}^{\mathcal{A}}(\omega; \omega, \Omega, -\Omega) = \mathbf{K}_{\text{mix}}^{\mathcal{A}(1)}(\omega; \omega, \Omega, -\Omega) + \mathbf{K}_{\text{mix}}^{\mathcal{A}(2)}(\omega; \omega, \Omega, -\Omega). \quad (\text{S84})$$

As in the previous cases, Eq. (S78) is evaluated at $T = 0$ with the sum over \mathbf{k} being performed numerically.

Antisymmetric susceptibility

The antisymmetric susceptibility, that mediates the light-induced Faraday effect, is found from the interaction kernels as

$$\chi_{xy}^{\mathcal{A}}(\omega; \omega, \Omega, -\Omega) = \frac{1}{\omega^2 \Omega^2} [\mathbf{K}_{\text{dia}}^{\mathcal{A}}(\omega; \omega, \Omega, -\Omega) + \mathbf{K}_{\text{para}}^{\mathcal{A}}(\omega; \omega, \Omega, -\Omega) + \mathbf{K}_{\text{mix}}^{\mathcal{A}}(\omega; \omega, \Omega, -\Omega)]. \quad (\text{S85})$$

The symmetric susceptibility χ_{xy}^S can be readily obtained from the kernel components derived above.

In the low-frequency limit, one finds that $\chi_{xy}^A(\omega; \omega, \Omega, -\Omega) \sim \omega\Omega$. This behavior demonstrates that the light-induced Faraday effect is intrinsically dynamical, vanishing in the limit of either a static pump or a static probe. On the other hand, one finds that $\chi_{xy}^S(\omega; \omega, \Omega, -\Omega)$ goes to a constant value for $\omega = 0$ and $\Omega = 0$. In Fig. S2 we show the ratio χ_{xy}^A/χ_{xy}^S for a fixed value of the probe frequency ω/Δ .

We emphasize that the derivation of the antisymmetric kernels in the diamagnetic, paramagnetic, and mixed cases does not rely on model-specific details. However, additional contributions to Eqs. (S65), (S73), and (S84) may arise in systems admitting nonvanishing mixed xy second-order vertices (or higher-order terms), whose presence depends on the specific structure of the tight-binding Hamiltonian $\mathcal{H}_{\mathbf{k}}$.

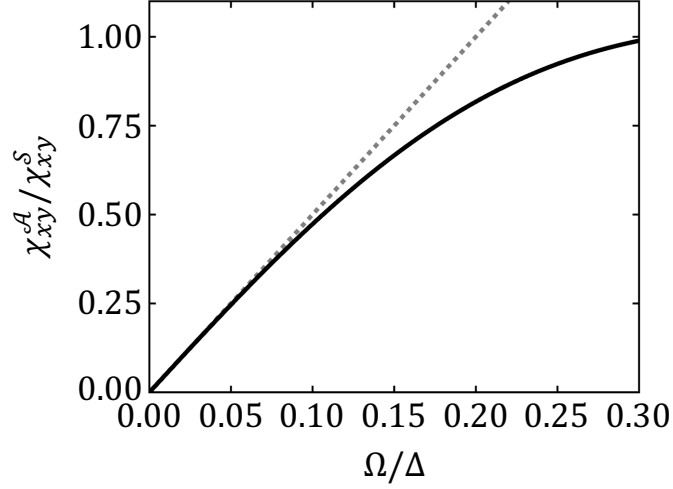


Figure S2. Ratio χ_{xy}^A/χ_{xy}^S in the sp -model as a function of the pump frequency Ω/Δ , for fixed probe frequency $\omega/\Delta = 1.5$ and for $t/\Delta = 0.1$. Gray dashed line follows the small-frequency linear behavior of the antisymmetric susceptibility.

DETAILS OF THE SIMULATIONS OF THE PUMP-PROBE RESPONSE WITH GAUSSIAN FIELDS

Here we detail the calculations and approximations considered to reproduce the pump-probe response spectrum shown in Fig. 3(d) of the main text.

To simulate a realistic response we must consider pump fields with finite bandwidths. In particular, we consider Gaussian pulses with a slight frequency mismatch:

$$\begin{aligned} E_{\text{pu}}^P(\omega_s) &= \mathcal{E}_P \mathcal{G}(\omega_s - \Omega + \Delta\Omega) + \mathcal{E}_P^* \mathcal{G}(\omega_s + \Omega - \Delta\Omega), \\ E_{\text{pu}}^S(\omega_s) &= \mathcal{E}_S \mathcal{G}(\omega_s - \Omega) + \mathcal{E}_S^* \mathcal{G}(\omega_s + \Omega), \end{aligned} \quad (\text{S86})$$

with

$$\mathcal{G}(\omega) = e^{-\frac{\omega^2 \tau^2}{2}}, \quad (\text{S87})$$

and τ represents the time duration of the pulse, which controls the bandwidth of the Gaussian pulse. We then closely follow the derivation below Eq. (S33), and change basis to \mathcal{E}_L and \mathcal{E}_R with Eqs. (S23). As we discussed above, only terms coming from the field combinations \mathcal{S}_\perp and \mathcal{A} of Eq. (S9) contribute to the differential dichroism $\Delta\Gamma_{R-L}$, which read for Gaussian pulses

$$\begin{aligned} \mathcal{S}_\perp &= -\frac{i}{2}(\mathcal{E}_L^2 - \mathcal{E}_R^2) [\mathcal{G}(\omega_2 - \Omega + \Delta\Omega)\mathcal{G}(\omega_3 - \Omega) + \mathcal{G}(\omega_2 - \Omega)\mathcal{G}(\omega_3 - \Omega + \Delta\Omega)] \\ &\quad + \frac{i}{2}(\mathcal{E}_L^{*2} - \mathcal{E}_R^{*2}) [\mathcal{G}(\omega_2 + \Omega - \Delta\Omega)\mathcal{G}(\omega_3 + \Omega) + \mathcal{G}(\omega_2 + \Omega)\mathcal{G}(\omega_3 + \Omega - \Delta\Omega)] \\ &\quad + \frac{i}{2}(|\mathcal{E}_L|^2 - |\mathcal{E}_R|^2) [\mathcal{G}(\omega_2 - \Omega + \Delta\Omega)\mathcal{G}(\omega_3 + \Omega) + \mathcal{G}(\omega_2 + \Omega)\mathcal{G}(\omega_3 - \Omega + \Delta\Omega) \\ &\quad - \mathcal{G}(\omega_2 - \Omega)\mathcal{G}(\omega_3 + \Omega - \Delta\Omega) - \mathcal{G}(\omega_2 + \Omega - \Delta\Omega)\mathcal{G}(\omega_3 - \Omega)], \end{aligned} \quad (\text{S88})$$

and

$$\begin{aligned} \mathcal{A} &= -\frac{i}{2}(\mathcal{E}_L^2 - \mathcal{E}_R^2) [\mathcal{G}(\omega_2 - \Omega + \Delta\Omega)\mathcal{G}(\omega_3 - \Omega) - \mathcal{G}(\omega_2 - \Omega)\mathcal{G}(\omega_3 - \Omega + \Delta\Omega)] \\ &\quad + \frac{i}{2}(\mathcal{E}_L^{*2} - \mathcal{E}_R^{*2}) [\mathcal{G}(\omega_2 + \Omega - \Delta\Omega)\mathcal{G}(\omega_3 + \Omega) - \mathcal{G}(\omega_2 + \Omega)\mathcal{G}(\omega_3 + \Omega - \Delta\Omega)] \\ &\quad + \frac{i}{2}(|\mathcal{E}_L|^2 - |\mathcal{E}_R|^2) [\mathcal{G}(\omega_2 - \Omega + \Delta\Omega)\mathcal{G}(\omega_3 + \Omega) + \mathcal{G}(\omega_2 - \Omega)\mathcal{G}(\omega_3 + \Omega - \Delta\Omega) \\ &\quad - \mathcal{G}(\omega_2 + \Omega)\mathcal{G}(\omega_3 - \Omega + \Delta\Omega) - \mathcal{G}(\omega_2 + \Omega - \Delta\Omega)\mathcal{G}(\omega_3 - \Omega)], \end{aligned} \quad (\text{S89})$$

where we have neglected terms in $\mathcal{E}_L \mathcal{E}_R^*$ and $\mathcal{E}_L^* \mathcal{E}_R$. Fixing $\theta = 0$ and $\Delta\theta = 0$, the relevant part of the differential intensity Eq. (S8) can be written as

$$\begin{aligned} \Delta\Gamma(t_{pp}, 0) &\propto \int d\omega_1 d\omega_2 d\omega_3 e^{-i(\omega_2 + \omega_3)t_{pp}} E_{\text{pr}}(\omega_1) [\chi_{xy}^S(\omega; \omega_1, \omega_2, \omega_3) \mathcal{S}_\perp + \chi_{xy}^A(\omega; \omega_1, \omega_2, \omega_3) \mathcal{A}] \\ &\simeq \frac{i}{2} \int d\omega_1 d\omega_2 d\omega_3 e^{-i(\omega_2 + \omega_3)t_{pp}} E_{\text{pr}}(\omega_1) \\ &\quad \times \left[-(\mathcal{E}_L^2 - \mathcal{E}_R^2) \chi_{xy}^S(\omega + 2\Omega; \omega, \Omega, \Omega) [\mathcal{G}(\omega_2 - \Omega + \Delta\Omega)\mathcal{G}(\omega_3 - \Omega) + \mathcal{G}(\omega_2 - \Omega)\mathcal{G}(\omega_3 - \Omega + \Delta\Omega)] \right. \\ &\quad + (\mathcal{E}_L^{*2} - \mathcal{E}_R^{*2}) \chi_{xy}^S(\omega - 2\Omega; \omega, -\Omega, -\Omega) [\mathcal{G}(\omega_2 + \Omega - \Delta\Omega)\mathcal{G}(\omega_3 + \Omega) + \mathcal{G}(\omega_2 + \Omega)\mathcal{G}(\omega_3 + \Omega - \Delta\Omega)] \\ &\quad + (|\mathcal{E}_L|^2 - |\mathcal{E}_R|^2) \chi_{xy}^S(\omega; \omega, \Omega, -\Omega) [\mathcal{G}(\omega_2 - \Omega + \Delta\Omega)\mathcal{G}(\omega_3 + \Omega) - \mathcal{G}(\omega_2 - \Omega)\mathcal{G}(\omega_3 + \Omega - \Delta\Omega) \\ &\quad + \mathcal{G}(\omega_2 + \Omega)\mathcal{G}(\omega_3 - \Omega + \Delta\Omega) - \mathcal{G}(\omega_2 + \Omega - \Delta\Omega)\mathcal{G}(\omega_3 - \Omega)] \\ &\quad + (|\mathcal{E}_L|^2 - |\mathcal{E}_R|^2) \chi_{xy}^A(\omega; \omega, \Omega, -\Omega) [\mathcal{G}(\omega_2 - \Omega + \Delta\Omega)\mathcal{G}(\omega_3 + \Omega) + \mathcal{G}(\omega_2 - \Omega)\mathcal{G}(\omega_3 + \Omega - \Delta\Omega) \\ &\quad \left. + \mathcal{G}(\omega_2 + \Omega)\mathcal{G}(\omega_3 - \Omega + \Delta\Omega) + \mathcal{G}(\omega_2 + \Omega - \Delta\Omega)\mathcal{G}(\omega_3 - \Omega)] \right]. \end{aligned} \quad (\text{S90})$$

In writing this expression, we evaluated the components of the susceptibility at the central frequencies of the pump (Ω and $\Omega - \Delta\Omega$) and probe (ω). This approximation is appropriate for narrowband pump pulses, $\Omega\tau \gg 1$, and is adopted to enable an efficient numerical evaluation of the response, as the integrals over ω_2 and ω_3 reduce to Gaussian

form. We then assume that $\chi_{xy}^S(\omega; \omega_1, \omega_2, \omega_3)$ is weakly dependent on the frequency arguments for small variations $\pm\Omega$ around the central frequency of the probe ω , and in particular approximately equivalent to $\chi_{xy}^S(\omega; \omega, \Omega, -\Omega)$. We can thus rewrite Eq. (S90) as

$$\begin{aligned} \Delta\Gamma(t_{pp}, 0) &\simeq \frac{i}{2} \chi_{xy}^S(\omega; \omega, \Omega, -\Omega) \int d\omega_1 d\omega_2 d\omega_3 e^{-i(\omega_2 + \omega_3)t_{pp}} E_{pr}(\omega_1) \\ &\times \left[-(\mathcal{E}_L^2 - \mathcal{E}_R^2)(\mathcal{G}(\omega_2 - \Omega + \Delta\Omega)\mathcal{G}(\omega_3 - \Omega) + \mathcal{G}(\omega_2 - \Omega)\mathcal{G}(\omega_3 - \Omega + \Delta\Omega)) \right. \\ &\quad + (\mathcal{E}_L^{*2} - \mathcal{E}_R^{*2})(\mathcal{G}(\omega_2 + \Omega - \Delta\Omega)\mathcal{G}(\omega_3 + \Omega) + \mathcal{G}(\omega_2 + \Omega)\mathcal{G}(\omega_3 + \Omega - \Delta\Omega)) \\ &\quad + (|\mathcal{E}_L|^2 - |\mathcal{E}_R|^2)(\mathcal{G}(\omega_2 - \Omega + \Delta\Omega)\mathcal{G}(\omega_3 + \Omega) - \mathcal{G}(\omega_2 - \Omega)\mathcal{G}(\omega_3 + \Omega - \Delta\Omega)) \\ &\quad + \mathcal{G}(\omega_2 + \Omega)\mathcal{G}(\omega_3 - \Omega + \Delta\Omega) - \mathcal{G}(\omega_2 + \Omega - \Delta\Omega)\mathcal{G}(\omega_3 - \Omega)) \\ &\quad + (|\mathcal{E}_L|^2 - |\mathcal{E}_R|^2) \frac{\chi_{xy}^A(\omega; \omega, \Omega, -\Omega)}{\chi_{xy}^S(\omega; \omega, \Omega, -\Omega)} (\mathcal{G}(\omega_2 - \Omega + \Delta\Omega)\mathcal{G}(\omega_3 + \Omega) + \mathcal{G}(\omega_2 - \Omega)\mathcal{G}(\omega_3 + \Omega - \Delta\Omega)) \\ &\quad \left. + \mathcal{G}(\omega_2 + \Omega)\mathcal{G}(\omega_3 - \Omega + \Delta\Omega) + \mathcal{G}(\omega_2 + \Omega - \Delta\Omega)\mathcal{G}(\omega_3 - \Omega) \right]. \end{aligned} \quad (\text{S91})$$

As it is the case for monochromatic pumps, the terms in $\mathcal{E}_L^2 - \mathcal{E}_R^2$ and $\mathcal{E}_L^{*2} - \mathcal{E}_R^{*2}$ contribute to the response centered at $\pm(2\Omega - \Delta\Omega)$, while terms in $|\mathcal{E}_L|^2 - |\mathcal{E}_R|^2$ contribute to the quasi-static response centered at $\pm\Delta\Omega$.

To explicitly calculate the response as in Fig. 3(d) of the main text, we fix the ratio $\chi_{xy}^A(\omega; \omega, \Omega, -\Omega)/\chi_{xy}^S(\omega; \omega, \Omega, -\Omega)$ to a reasonable value obtained from calculations in the *sp*-model, and we take a narrowband Gaussian probe field with central frequency $\omega \gg \Omega$. The Fourier-transformed dichroic signal $\Delta\bar{\Gamma}_{R-L}(\omega_{pp}, 0)$ obtained from Eq. (S91) provides the full pump-probe response, while the symmetric response is obtained neglecting the antisymmetric contribution.

PHONON-MEDIATED ANTISYMMETRIC RESPONSE

Electron-phonon interaction and linear phonon excitation

We here compute the antisymmetric susceptibility that mediates the light-induced Faraday effect in presence of IR-active phonons driven by the pump field. By definition, in the dipole approximation an IR-active phonon \mathbf{Q} transforms as a polar vector, and thus can be treated on the same footing as the vector potential \mathbf{A} . In the path-integral formalism, the system is described by $\mathcal{Z} = \int \mathcal{D}[\psi] \mathcal{D}[\mathbf{A}] \mathcal{D}[\mathbf{Q}] e^{-S[\psi, \mathbf{A}, \mathbf{Q}]}$, where the light-matter action reads

$$S[\psi, \mathbf{A}, \mathbf{Q}] = - \sum_{i\nu_n, \mathbf{k}} \psi_{\mathbf{k}}^T(-i\nu_n) \tilde{G}_0^{-1}(i\nu_n, \mathbf{k}) \psi_{\mathbf{k}}(i\nu_n) + \sum_{i\nu_n, \mathbf{k}} \sum_{i\nu'_n, \mathbf{k}'} \psi_{\mathbf{k}}^T(-i\nu_n) \Sigma_{\mathbf{k}\mathbf{k}'}(i\nu_n - i\nu'_n) \psi_{\mathbf{k}'}(i\nu'_n) - \sum_{i\Omega_m} \frac{\Omega_m^2 + \omega_0^2(T)}{2\omega_0(T)} |\mathbf{Q}(i\Omega_m)|^2, \quad (\text{S92})$$

where

$$\Sigma_{\mathbf{k}\mathbf{k}'}(i\nu_n - i\nu'_n) \simeq \delta_{\mathbf{k}\mathbf{k}'} \left[\sqrt{\frac{T}{N}} \frac{e}{c} \sum_{i\Omega_m} [\tilde{v}_x A_x(i\Omega_m) + \tilde{v}_y A_y(i\Omega_m)] \delta(i\Omega_m - i\nu_n + i\nu'_n) + \frac{T}{N} \frac{e^2}{2c^2} \sum_{i\Omega_m} \sum_{i\Omega_n} [\tilde{\rho}_x A_x(i\Omega_m) A_x(i\Omega_n) + \tilde{\rho}_y A_y(i\Omega_m) A_y(i\Omega_n)] \delta(i\Omega_m + i\Omega_n - i\nu_n + i\nu'_n) + \sqrt{\frac{T}{N}} \sum_{i\Omega_m} [\tilde{g}_x Q_x(i\Omega_m) + \tilde{g}_y Q_y(i\Omega_m)] \delta(i\Omega_m - i\nu_n + i\nu'_n) + \frac{T}{N} \frac{e}{c} \sum_{i\Omega_m} \sum_{i\Omega_n} [\tilde{h}_x Q_x(i\Omega_m) A_x(i\Omega_n) + \tilde{h}_y Q_y(i\Omega_m) A_y(i\Omega_n)] \delta(i\Omega_m + i\Omega_n - i\nu_n + i\nu'_n) \right]. \quad (\text{S93})$$

In particular, the $|\mathbf{Q}|^2$ term in the second row of Eq. (S92) describes the bare phonon, which we take dispersionless at a temperature-dependent frequency $\omega_0(T)$. The coefficients \tilde{g}_i , written in the orbital basis, mediate the electron-phonon interactions, while \tilde{h}_i represent mixed phonon-photon vertices. The transverse-optical IR-active phonon of the sp -model results in electron-phonon vertices \tilde{g}_i and \tilde{h}_i with a similar matrix structure to the paramagnetic (\tilde{v}_i) and diamagnetic ($\tilde{\rho}_i$) light-matter couplings of the purely electronic model, respectively. In writing Eq. (S93) we have immediately neglected terms that do not contribute to the two-phonon susceptibility $\chi_{xy}^{A, \text{ph}}$ shown in Fig. 4(a) of the main text. For example, terms corresponding to two-phonon-mediated electronic transitions $\sim \psi Q_x Q_x \psi$ and $\sim \psi Q_y Q_y \psi$ are only relevant when the fields can directly excite two phonons with the same polarization. However, the probe is assumed at a much higher frequency with respect to the characteristic phonon frequency, and we are interested in components of the susceptibility with mixed pump indices, $\chi_{xy;xy}$ and $\chi_{xy;yx}$, so that these vertices do not enter in the calculations. On the other hand, we neglect terms mixing x and y components at the same vertex, $\sim \psi Q_x Q_y \psi$, consistently with the structure of the electron-photon interaction obtained within the sp -model. We then integrate the electron field out of the partition function, and find the effective action that couples the electromagnetic field to the phonon field:

$$S_{\text{eff}}[\mathbf{A}, \mathbf{Q}] = \sum_{m \geq 1} \frac{\text{Tr}[\tilde{G}_0 \Sigma]^m}{m} - \sum_{i\Omega_m} \frac{\Omega_m^2 + \omega_0^2(T)}{2\omega_0(T)} |\mathbf{Q}(i\Omega_m)|^2. \quad (\text{S94})$$

The relevant processes needed to calculate the phonon-mediated diagram are shown in Fig. S3. We first focus on the linear couplings $Q_x A_x$ and $Q_y A_y$, that encode the direct excitation of the phonons via the pump fields. Subsequently, we evaluate the nonlinear electronic 4-point loop Π_{xy}^A , composed by the terms scaling with $Q_x Q_y A_x A_y$, that describe mixed third-order processes with two phonons and two photons. As in the electronic case, we can distinguish between diamagnetic, paramagnetic, and mixed contributions.

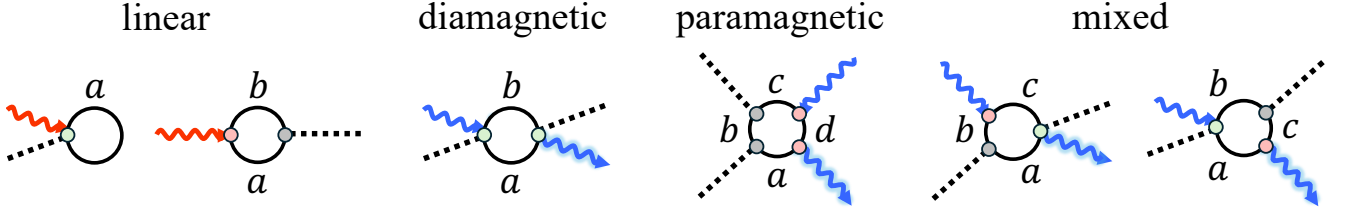


Figure S3. Diagrammatic representation of the processes contributing to the phonon-mediated diagram depicted in Fig. 4(a) of the main text. Red wavy lines denote the pump fields, Blue wavy lines denote the probe field, black dashed lines denote the phonon. Black solid lines represent electronic propagators. Red dots denote velocity vertices, gray dots represent the electron-phonon vertices, and green dots denote the mixed phonon-photon vertices. The probe photon on which the detection is performed is highlighted with a blue shadow.

Linear coupling

The linear couplings $Q_x A_x$ and $Q_y A_y$ are contained in the $m = 1$ and $m = 2$ terms of the expansion, and read

$$\begin{aligned}
S_c[\mathbf{A}, \mathbf{Q}] &= \frac{e}{c} \sum_{i\Omega_m} \sum_{i=x,y} \frac{T}{N} \sum_{i\nu_n, \mathbf{k}} \text{Tr}[\tilde{G}_0(i\nu_n, \mathbf{k}) \tilde{h}_i] A_i(i\Omega_m) Q_i(-i\Omega_m) \\
&+ \frac{e}{c} \sum_{i\Omega_m} \sum_{i,j=x,y} \frac{T}{N} \sum_{i\nu_n, \mathbf{k}} \text{Tr}[\tilde{G}_0(i\nu_n, \mathbf{k}) \tilde{v}_i \tilde{G}_0(i\nu_n + i\Omega_m, \mathbf{k}) \tilde{g}_j] A_i(i\Omega_m) Q_j(-i\Omega_m) \\
&= \frac{e}{c} \sum_{i\Omega_m} \sum_{i=x,y} \frac{T}{N} \sum_{i\nu_n, \mathbf{k}} \text{Tr}[G_0(i\nu_n, \mathbf{k}) h_i] A_i(i\Omega_m) Q_i(-i\Omega_m) \\
&+ \frac{e}{c} \sum_{i\Omega_m} \sum_{i,j=x,y} \frac{T}{N} \sum_{i\nu_n, \mathbf{k}} \text{Tr}[G_0(i\nu_n, \mathbf{k}) v_i G_0(i\nu_n + i\Omega_m, \mathbf{k}) g_j] A_i(i\Omega_m) Q_j(-i\Omega_m), \tag{S95}
\end{aligned}$$

where, following the notation defined above, $g_i = U_{\mathbf{k}}^\dagger \tilde{g}_i U_{\mathbf{k}}$ and $h_i = U_{\mathbf{k}}^\dagger \tilde{h}_i U_{\mathbf{k}}$ represent the electron-phonon vertices in the band basis. We can thus define

$$Z_{ij}(i\Omega_m) = e \left[\frac{T}{N} \sum_{i\nu_n, \mathbf{k}} \text{Tr}[G_0(i\nu_n, \mathbf{k}) h_i] + \frac{T}{N} \sum_{i\nu_n, \mathbf{k}} \text{Tr}[G_0(i\nu_n, \mathbf{k}) v_i G_0(i\nu_n + i\Omega_m, \mathbf{k}) g_j] \right], \tag{S96}$$

so that the action of the linear coupling becomes

$$S_c[\mathbf{A}, \mathbf{Q}] = \frac{1}{c} \sum_{i,j=x,y} \sum_{i\Omega_m} Z_{ij}(i\Omega_m) A_i(i\Omega_m) Q_j(-i\Omega_m). \tag{S97}$$

In the following we consider an isotropic and frequency-independent coupling, $Z_{ij}(i\Omega_m) = Z \delta_{ij}$. We note that the quantity Z here defined is linked to the usual Born effective charge Z_B as $Z_B = Z \sqrt{M/\omega_0(T)}$, with M the ionic mass [34].

Diamagnetic-like phonon-mediated antisymmetric kernel

The diamagnetic-like contribution is contained in the $m = 2$ term of $S_{\text{eff}}[\mathbf{A}, \mathbf{Q}]$ in Eq. (S94), when multiplying twice the fourth row of Eq. (S93). In particular,

$$\begin{aligned}
S_{\text{dia}}[\mathbf{A}, \mathbf{Q}] &= \frac{e^2}{c^2} \sum_{i\Omega_m} \sum_{i\Omega_n} \sum_{i\Omega_l} \sum_{i\Omega_s} \frac{T}{N} \sum_{i\nu_n, \mathbf{k}} \text{Tr}[\tilde{G}_0(i\nu_n, \mathbf{k}) \tilde{h}_y \tilde{G}_0(i\nu_n + i\Omega_m + i\Omega_n, \mathbf{k}) \tilde{h}_x] \\
&\quad \times Q_y(i\Omega_m) A_y(i\Omega_m) Q_x(i\Omega_l) A_x(i\Omega_s) \delta_{-i\Omega_s, i\Omega_m + i\Omega_n + i\Omega_l}, \tag{S98}
\end{aligned}$$

where $i\Omega_m + i\Omega_n + i\Omega_l + i\Omega_s = 0$ by energy conservation. Following the same derivation detailed below Eq. (S58), the two components of the diamagnetic kernel read

$$\mathbf{K}_{xy;yx}^{\text{dia,ph}}(\omega; \omega, \Omega, -\Omega) = -\frac{e^2}{2} \sum_{ab} [h_y]_{ab} [h_x]_{ba} d_{ab}(\omega + \Omega), \quad (\text{S99})$$

and

$$\mathbf{K}_{xy;xy}^{\text{dia,ph}}(\omega; \omega, \Omega, -\Omega) = -\frac{e^2}{2} \sum_{ab} [h_y]_{ab} [h_x]_{ba} d_{ab}(\omega - \Omega), \quad (\text{S100})$$

where d_{ab} is defined as in Eq. (S61). In this way, the antisymmetric diamagnetic component reads

$$\mathbf{K}_{\text{dia}}^{\text{A,ph}}(\omega; \omega, \Omega, -\Omega) = -\frac{e^2}{2} \sum_{ab} [[h_x]_{ab} [h_y]_{ba} + [h_y]_{ab} [h_x]_{ba}] [d_{ab}(\omega - \Omega) - d_{ab}(\omega + \Omega)]. \quad (\text{S101})$$

Paramagnetic-like phonon-mediated antisymmetric kernel

The paramagnetic-like contribution is contained in the $m = 4$ term of $S_{\text{eff}}[\mathbf{A}, \mathbf{Q}]$ in Eq. (S94), when multiplying twice the first row with twice the third row of Eq. (S93). In particular,

$$\begin{aligned} S_{\text{para}}[\mathbf{A}, \mathbf{Q}] &= \frac{e^2}{4c^2} \sum_{i\Omega_m} \sum_{i\Omega_n} \sum_{i\Omega_l} \sum_{i\Omega_s} \\ &\frac{T}{N} \sum_{i\nu_n, \mathbf{k}} \text{Tr} [\tilde{G}_0(i\nu_n, \mathbf{k}) \tilde{g}_y \tilde{G}_0(i\nu_n + i\Omega_m, \mathbf{k}) \tilde{v}_y \tilde{G}_0(i\nu_n + i\Omega_m + i\Omega_n, \mathbf{k}) \tilde{g}_x \tilde{G}_0(i\nu_n + i\Omega_m + i\Omega_n + i\Omega_l, \mathbf{k}) \tilde{v}_x] \\ &\times \mathbf{Q}_y(i\Omega_m) \mathbf{A}_y(i\Omega_n) \mathbf{Q}_x(i\Omega_l) \mathbf{A}_x(i\Omega_s) \delta_{-i\Omega_s, i\Omega_m + i\Omega_n + i\Omega_l} + \text{perm.}, \end{aligned} \quad (\text{S102})$$

where ‘‘perm.’’ denotes all distinct permutations of the external field insertions, i.e., all possible ways of attaching the photon and phonon legs to the fermionic loop. Following the same derivation detailed below Eq. (S66), the two components of the paramagnetic kernel read

$$\begin{aligned} \mathbf{K}_{xy;yx}^{\text{para,ph}}(\omega; \omega, \Omega, -\Omega) &= -\frac{e^2}{4} \sum_{abcd} \left[[v_y]_{ab} [g_y]_{bc} [g_x]_{cd} [v_x]_{da} p_{abcd}(\omega, \Omega, -\Omega) \right. \\ &\quad + [g_y]_{ab} [v_y]_{bc} [g_x]_{cd} [v_x]_{da} p_{abcd}(\Omega, \omega, -\Omega) \\ &\quad + [g_x]_{ab} [g_y]_{bc} [v_y]_{cd} [v_x]_{da} p_{abcd}(-\Omega, \Omega, \omega) \\ &\quad + [g_x]_{ab} [v_y]_{bc} [g_y]_{cd} [v_x]_{da} p_{abcd}(-\Omega, \omega, \Omega) \\ &\quad + [g_y]_{ab} [g_x]_{bc} [v_y]_{cd} [v_x]_{da} p_{abcd}(\Omega, -\Omega, \omega) \\ &\quad \left. + [v_y]_{ab} [g_x]_{bc} [g_y]_{cd} [v_x]_{da} p_{abcd}(\omega, -\Omega, \Omega) \right], \end{aligned} \quad (\text{S103})$$

and

$$\begin{aligned} \mathbf{K}_{xy;xy}^{\text{para,ph}}(\omega; \omega, \Omega, -\Omega) &= -\frac{e^2}{4} \sum_{abcd} \left[[v_y]_{ab} [g_x]_{bc} [g_y]_{cd} [v_x]_{da} p_{abcd}(\omega, \Omega, -\Omega) \right. \\ &\quad + [g_x]_{ab} [v_y]_{bc} [g_y]_{cd} [v_x]_{da} p_{abcd}(\Omega, \omega, -\Omega) \\ &\quad + [g_y]_{ab} [g_x]_{bc} [v_y]_{cd} [v_x]_{da} p_{abcd}(-\Omega, \Omega, \omega) \\ &\quad + [g_y]_{ab} [v_y]_{bc} [g_x]_{cd} [v_x]_{da} p_{abcd}(-\Omega, \omega, \Omega) \\ &\quad + [g_x]_{ab} [g_y]_{bc} [v_y]_{cd} [v_x]_{da} p_{abcd}(\Omega, -\Omega, \omega) \\ &\quad \left. + [v_y]_{ab} [g_y]_{bc} [g_x]_{cd} [v_x]_{da} p_{abcd}(\omega, -\Omega, \Omega) \right], \end{aligned} \quad (\text{S104})$$

where p_{abcd} is defined as in Eq. (S69). Notice that we have fixed the detection on an x photon field, which fixes the last matrix element $[v_x]_{da}$. By defining the vectors $\mathbf{v} = (v_x, v_y)$ and $\mathbf{g} = (g_x, g_y)$, the antisymmetric paramagnetic

component can be written in a compact way as

$$\begin{aligned} K_{\text{para}}^{\mathcal{A},\text{ph}}(\omega; \omega, \Omega, -\Omega) = & -\frac{e^2}{8} \sum_{abcd} [([\mathbf{g}]_{ab} \times [\mathbf{g}]_{bc}) \cdot ([\mathbf{v}]_{cd} \times [\mathbf{v}]_{da})] [p_{abcd}(-\Omega, \Omega, \omega) - p_{abcd}(\Omega, -\Omega, \omega)] \\ & + [([\mathbf{g}]_{ab} \times [\mathbf{g}]_{cd}) \cdot ([\mathbf{v}]_{bc} \times [\mathbf{v}]_{da})] [p_{abcd}(-\Omega, \omega, \Omega) - p_{abcd}(\Omega, \omega, -\Omega)] \\ & + [([\mathbf{g}]_{bc} \times [\mathbf{g}]_{cd}) \cdot ([\mathbf{v}]_{ab} \times [\mathbf{v}]_{da})] [p_{abcd}(\omega, -\Omega, \Omega) - p_{abcd}(\omega, \Omega, -\Omega)]. \end{aligned} \quad (\text{S105})$$

Mixed diamagnetic-paramagnetic phonon-mediated antisymmetric kernel

The mixed diamagnetic-paramagnetic contributions are contained in the $m = 3$ term of $S_{\text{eff}}[\mathbf{A}, \mathbf{Q}]$ in Eq. (S94), when multiplying the first, the third, and the fourth row of Eq. (S93). In particular, we can distinguish between two contributions,

$$\begin{aligned} S_{\text{mix}}^{(1)}[\mathbf{A}, \mathbf{Q}] = & \frac{e^2}{3c^2} \sum_{i\Omega_m} \sum_{i\Omega_n} \sum_{i\Omega_l} \sum_{i\Omega_s} \frac{T}{N} \sum_{i\nu_n, \mathbf{k}} \text{Tr}[\tilde{G}_0(i\nu_n, \mathbf{k}) \tilde{g}_y \tilde{G}_0(i\nu_n + i\Omega_m, \mathbf{k}) \tilde{v}_y \tilde{G}_0(i\nu_n + i\Omega_m + i\Omega_n, \mathbf{k}) \tilde{h}_x] \\ & \times Q_y(i\Omega_m) A_y(i\Omega_n) Q_x(i\Omega_l) A_x(i\Omega_s) \delta_{-i\Omega_s, i\Omega_m + i\Omega_n + i\Omega_l}, \end{aligned} \quad (\text{S106})$$

corresponding to a detection performed on a diamagnetic insertion, and

$$\begin{aligned} S_{\text{mix}}^{(2)}[\mathbf{A}, \mathbf{Q}] = & \frac{e^2}{3c^2} \sum_{i\Omega_m} \sum_{i\Omega_n} \sum_{i\Omega_l} \sum_{i\Omega_s} \frac{T}{N} \sum_{i\nu_n, \mathbf{k}} \text{Tr}[\tilde{G}_0(i\nu_n, \mathbf{k}) \tilde{h}_y \tilde{G}_0(i\nu_n + i\Omega_m + i\Omega_n, \mathbf{k}) \tilde{g}_y \tilde{G}_0(i\nu_n + i\Omega_m + i\Omega_n + i\Omega_l, \mathbf{k}) \tilde{v}_x] \\ & \times Q_y(i\Omega_m) A_y(i\Omega_n) Q_x(i\Omega_l) A_x(i\Omega_s) \delta_{-i\Omega_s, i\Omega_m + i\Omega_n + i\Omega_l}, \end{aligned} \quad (\text{S107})$$

corresponding to a detection performed on a paramagnetic insertion. Following the same derivation detailed below Eqs. (S74) and (S75), one finds the antisymmetric contributions coming from these two actions, that read

$$K_{\text{mix}}^{\mathcal{A}(1),\text{ph}}(\omega; \omega, \Omega, -\Omega) = -\frac{e^2}{6} \sum_{abc} [[v_x]_{ab} [g_x]_{bc} [h_y]_{ca} + [v_y]_{ab} [g_y]_{bc} [h_x]_{ca}] [m_{abc}(\omega, \omega - \Omega) - m_{abc}(\omega, \omega + \Omega)], \quad (\text{S108})$$

and

$$K_{\text{mix}}^{\mathcal{A}(2),\text{ph}}(\omega; \omega, \Omega, -\Omega) = -\frac{e^2}{6} \sum_{abc} [[h_x]_{ab} [g_x]_{bc} [v_y]_{ca} + [h_y]_{ab} [g_y]_{bc} [v_x]_{ca}] [m_{abc}(\omega - \Omega, \omega) - m_{abc}(\omega + \Omega, \omega)], \quad (\text{S109})$$

where m_{abc} is defined as in Eq. (S78). The total mixed diamagnetic-paramagnetic antisymmetric kernel is then found as

$$K_{\text{mix}}^{\mathcal{A},\text{ph}}(\omega; \omega, \Omega, -\Omega) = K_{\text{mix}}^{\mathcal{A}(1),\text{ph}}(\omega; \omega, \Omega, -\Omega) + K_{\text{mix}}^{\mathcal{A}(2),\text{ph}}(\omega; \omega, \Omega, -\Omega). \quad (\text{S110})$$

Antisymmetric phonon-mediated susceptibility

The total antisymmetric electronic loop reads

$$\Pi_{xy}^{\mathcal{A}}(\omega; \omega, \Omega, -\Omega) = \frac{1}{\omega^2 \Omega^2} [K_{\text{dia}}^{\mathcal{A},\text{ph}}(\omega; \omega, \Omega, -\Omega) + K_{\text{para}}^{\mathcal{A},\text{ph}}(\omega; \omega, \Omega, -\Omega) + K_{\text{mix}}^{\mathcal{A},\text{ph}}(\omega; \omega, \Omega, -\Omega)]. \quad (\text{S111})$$

This response function does not by itself represent a physical optical response, as it requires two phonon insertions. The corresponding response function for the process shown in Fig. 4(a) of the main text is obtained by attaching the phonon propagators to two pump photons via the linear coupling in Eq. (S97), and integrating the phonon field out of the partition function. In this way, one finally finds

$$\chi_{xy}^{\mathcal{A},\text{ph}}(\omega; \omega, \Omega, -\Omega) = Z^2 D(\Omega) D(-\Omega) \Pi_{xy}^{\mathcal{A}}(\omega; \omega, \Omega, -\Omega), \quad (\text{S112})$$

where

$$D(\Omega) = \frac{2\omega_0(T)}{(\Omega + i0^+)^2 - \omega_0^2(T)} \quad (\text{S113})$$

is the bare-phonon propagator. Eq. (S112) corresponds to Eq. (13) of the main text, once a temperature-dependent phenomenological damping parameter $\gamma(T)$ is introduced in the phonon propagator to describe its inverse lifetime.

The symmetric electronic loop $\Pi_{xy}^{\mathcal{S}}$, and the corresponding optical response function $\chi_{xy}^{\mathcal{S}}$, can be readily obtained from the kernel components derived above with analogous calculations.

Relative magnitude between all-electronic and phonon-mediated processes

The relative magnitude between the fully electronic process described by χ_{xy}^A in Eq. (S85) and the phonon-mediated contribution described by $\chi_{xy}^{A,\text{ph}}$ in Eq. (S112) can be estimated from their ratio. We take the Fermi velocity v_F as the characteristic magnitude scale of the velocity vertices, while the electron-phonon vertex scales as $\beta v_F \sqrt{\frac{1}{M\omega_0(T)}}$ [34], where β is a dimensionless parameterization of the electron-phonon coupling strength. One then finds

$$\frac{\chi_{xy}^{A,\text{ph}}(\omega; \omega, \Omega, -\Omega)}{\chi_{xy}^A(\omega; \omega, \Omega, -\Omega)} \sim \frac{\alpha v_F^2 \left(\beta v_F \sqrt{\frac{1}{M\omega_0(T)}} \right)^2 Z^2}{v_F^4} D(\Omega) D(-\Omega) = \frac{\alpha \beta^2 Z^2}{M\omega_0(T)} D(\Omega) D(-\Omega), \quad (\text{S114})$$

where α is a dimensionless constant of order 1. Introducing the Born effective charge as $Z = Z_B \sqrt{\frac{\omega_0(T)}{M}}$, we obtain

$$\frac{\chi_{xy}^{A,\text{ph}}(\omega; \omega, \Omega, -\Omega)}{\chi_{xy}^A(\omega; \omega, \Omega, -\Omega)} \sim \frac{\alpha \beta^2 Z_B^2}{M^2} D(\Omega) D(-\Omega). \quad (\text{S115})$$

An *ab-initio* estimate of the ionic mass M , the electron-phonon coupling β and the Born effective charge Z_B would therefore provide a quantitative estimate of the relative strength between the two processes. In the main text, we use $\sqrt{\alpha} \beta Z_B / M = 0.06 \Omega$, which is of the correct order of magnitude of what expected in SrTiO₃. Spectra reported in Fig. 4 of the main text are obtained with Gaussian pulses, following calculations analogous to those discussed below Eq. (S86).